# Diurnal cycle of tropical precipitation in a general circulation model

J. Craig Collier and Kenneth P. Bowman

Department of Atmospheric Sciences, Texas A & M University, College Station, Texas, USA

Received 25 March 2004; revised 16 June 2004; accepted 29 June 2004; published 14 September 2004.

[1] Hourly averaged precipitation rates from an ensemble of the Community Climate Model version 3 (CCM3) simulations for the 44-month period from January 1998 through August 2001 are compared to observations from the Tropical Rainfall Measuring Mission (TRMM) satellite. In order to have adequate sampling by the satellite, comparisons are made for 15° longitude × 10° latitude boxes and for larger geographical areas within the tropics. The temporally and spatially averaged hourly precipitation rates from CCM3 and from TRMM are fit to the diurnal harmonic by the method of linear least squares regression, and the phases and the amplitudes of the diurnal cycles are compared. The model's diurnal cycle is too strong over major land masses, particularly over South America (200% too large), and is too weak over many oceans, particularly the northwestern tropical Pacific (57% too small). The model-satellite phase differences tend to be more homogeneous. The peak in the model's diurnal harmonic consistently precedes that of the observations nearly everywhere. Phase differences are large over Australia, Papua New Guinea, and Saharan Africa, where CCM3 leads TRMM by 4 hours, 5 to 6 hours, and 9 to 11 hours, respectively. The model's phase and amplitude biases likely have effects on its hydrologic cycle and its surface and atmospheric energy budgets. Thus the causes for the model's biases need to be investigated. *INDEX TERMS:* 1610 Global Change: Atmosphere (0315, 0325); 3354 Meteorology and Atmospheric Dynamics: Precipitation (1854); 3337 Meteorology and Atmospheric Dynamics: Numerical modeling and data assimilation; *KEYWORDS:* diurnal, precipitation, general, circulation, model, GCM

**Citation:** Collier, J. C., and K. P. Bowman (2004), Diurnal cycle of tropical precipitation in a general circulation model, *J. Geophys. Res.*, *109*, D17105, doi:10.1029/2004JD004818.

## 1. Introduction

[2] Many previous studies have investigated the diurnal cycle of precipitation and/or convection over ocean and over land, as measured by various Earth-observing systems. Well over 100 studies document the phenomenon [*Wallace*, 1975]. While these studies generally agree that the magnitude of the diurnal cycle is larger over the continents than over the oceans, several also show that land regions exhibit maxima in precipitation between noon and midnight while ocean regions have maxima between midnight and noon. In tropical latitudes, these studies include analyses of surface-based measurements from island and continental stations from the tropical west Pacific to South America and Africa [*Gray and Jacobson*, 1977]; reflectivity and microwave data from the Tropical Rainfall Measuring Mission (TRMM) satellite [*Nesbitt and Zipser*, 2003]; infrared, passive microwave, and gauge data [*Janowiak et al.*, 1994]; infrared data from American geostationary satellites [*Meisner and Arkin*, 1987]; microwave data from the Defense Meteorological Satellite Program (DMSP) satellite [*Sharma et al.*, 1991]; and gauge data from the Tropical Atmosphere Ocean (TAO) mooring array for the Coupled Ocean Atmosphere Response Experiment (COARE) [*Cronin and McPhaden*, 1999]. However, regional exceptions have been found (e.g., the eastern Atlantic [*McGarry and Reed*, 1978; *Reed and Jaffe*, 1981], the southern Pacific and Atlantic Ocean dry zones [*Chang et al.*, 1995], and the South Pacific Convergence Zone (SPCZ) [*Albright et al.*, 1985]. In addition, the diurnal variation itself can depend on the intensity of precipitation (i.e., drizzle versus thunderstorms) [*Dai*, 2001].

[3] As observational studies abound, so do studies on the causes of the diurnal cycle of precipitation and why it varies geographically and, in general, from land to ocean. According to *Wallace* [1975], the theories for the diurnal cycle of convectively based precipitation over land can fall into one of two categories. The first consists of theories based on thermodynamic processes which affect static stability; the second groups together theories which explain the diurnal cycle of convection by dynamical processes affecting convergence in the boundary layer, such as the land and sea breeze circulations in coastal areas. For the oceanic diurnal cycle, theories have been proposed by *Kraus* [1963], *Brier and Simpson* [1969], and *Gray and Jacobson* [1977], among others and are summarized nicely by *Nesbitt and Zipser* [2003]. The cause for the morning peak remains


0148-0227/04/2004JD004818$09.00

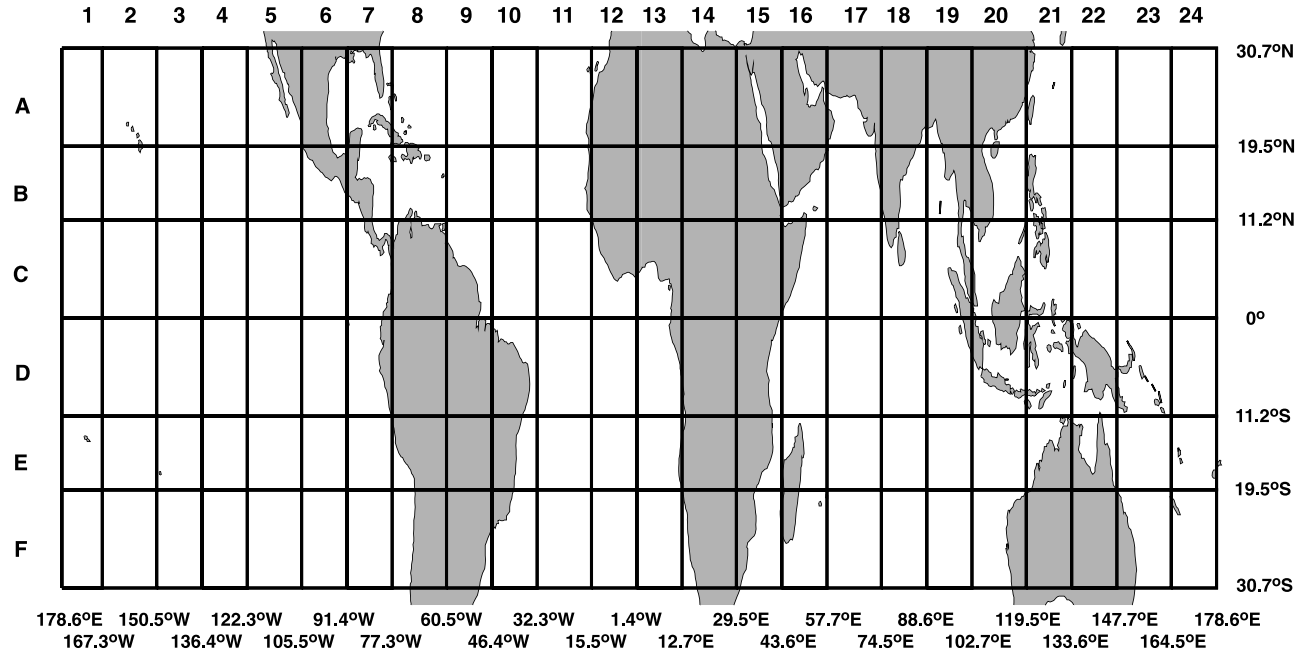


**Figure 1.** Map of the 144 regions used for the diurnal cycle comparison. Climatological mean hourly precipitation rates from Community Climate Model version 3 (CCM3) and from Tropical Rainfall Measuring Mission (TRMM) are averaged over each of the above regions. Note that the grid appears irregular because the region boundaries were chosen to line up with the model's grid, which is irregularly spaced.

widely debated. The diurnal cycle of precipitation is also intrinsically interesting. Observing the natural variation of rainfall throughout a day helps scientists better understand convective processes.

[4] General circulation models (GCMs) may be used for making predictions of long-term trends in precipitation, and agreement between model-simulated and observed precipitation on long timescales has been the subject of previous studies (see *Chen et al.* [1996], *Latif et al.* [2001], *Kirkyla and Hameed* [1989], and *Collier et al.* [2004], among others). However, general circulation models should simulate accurate monthly mean precipitation amounts for the right reasons [*Trenberth et al.*, 2003], simulating the local timing correctly. A variety of studies have used observations of the diurnal cycle to compare with modeling results. Examples include analysis of output from the Colorado State University General Circulation Model over tropical lands and oceans [*Randall et al.*, 1991] and over South America [*Lin et al.*, 2000], output from the NCAR Community Climate Model version 2 (CCM2) [*Chen et al.*, 1996] and CCM3 [*Dai et al.*, 1999] over the United States, output from the NCAR Community Climate System Model version 2 (CCSM2) [*Dai and Trenberth*, 2004], and output from the European Centre for Medium-Range Weather Forecasts (ECMWF) model over Amazonia [*Betts and Jakob*, 2002a, 2002b]. Our study compares the GCM-simulated and observed diurnal cycles of precipitation on large space scales in the tropics. We take advantage of tropical rainfall data provided by the Tropical Rainfall Measuring Mission (TRMM) satellite to verify the diurnal cycle of precipitation as simulated by the National Center for Atmospheric Research (NCAR) Community Climate Model (CCM3) over a 44-month period from 1998 to 2001. Spatially and temporally averaged hourly rain rates are fit to a diurnal harmonic. We intend to focus on the geographical distribution of areas of agreement and disagreement.

## 2. Methods

### 2.1. TRMM Data

[5] This study uses the TRMM 3G68 data set, which was obtained from the TRMM Science Data and Information System (TSDIS). It consists of essentially instantaneous precipitation rates derived from TMI, from PR, and from the combination of both instruments averaged over $0.5^\circ \times 0.5^\circ$ latitude-longitude boxes between 38°S and 38°N. A complete description of the satellite and its instruments of rainfall measurement are given by *Kummerow et al.* [1998, 2000]. For validating CCM3, we use the precipitation rates from the combination of TMI and PR. Generally, the TRMM satellite is able to observe a given location in the tropics about once per day, at a different time each day, with a cycle of 46 days, the period of its orbital precession [*Negri and Bell*, 2002]. Therefore, for the 44-month period considered here (January 1998 to August 2001), there are about 1320 observations of each of the aforementioned boxes. For each box, we estimate there to be about 28 samples of any particular hour. Precipitation is highly variable in both space and time, and the incomplete nature of the satellite's sampling introduces an error in the retrieval relative to actual ground truth. This error is known as sampling error and has been the subject of several studies [see, e.g., *Shin and North*, 1988; *Bell and Kundu*, 1996, 2000; *Bell et al.*, 2001; *Bell and Kundu*, 2003; K. P. Bowman, Comparison of TRMM precipitation retrievals with rain gauge data from

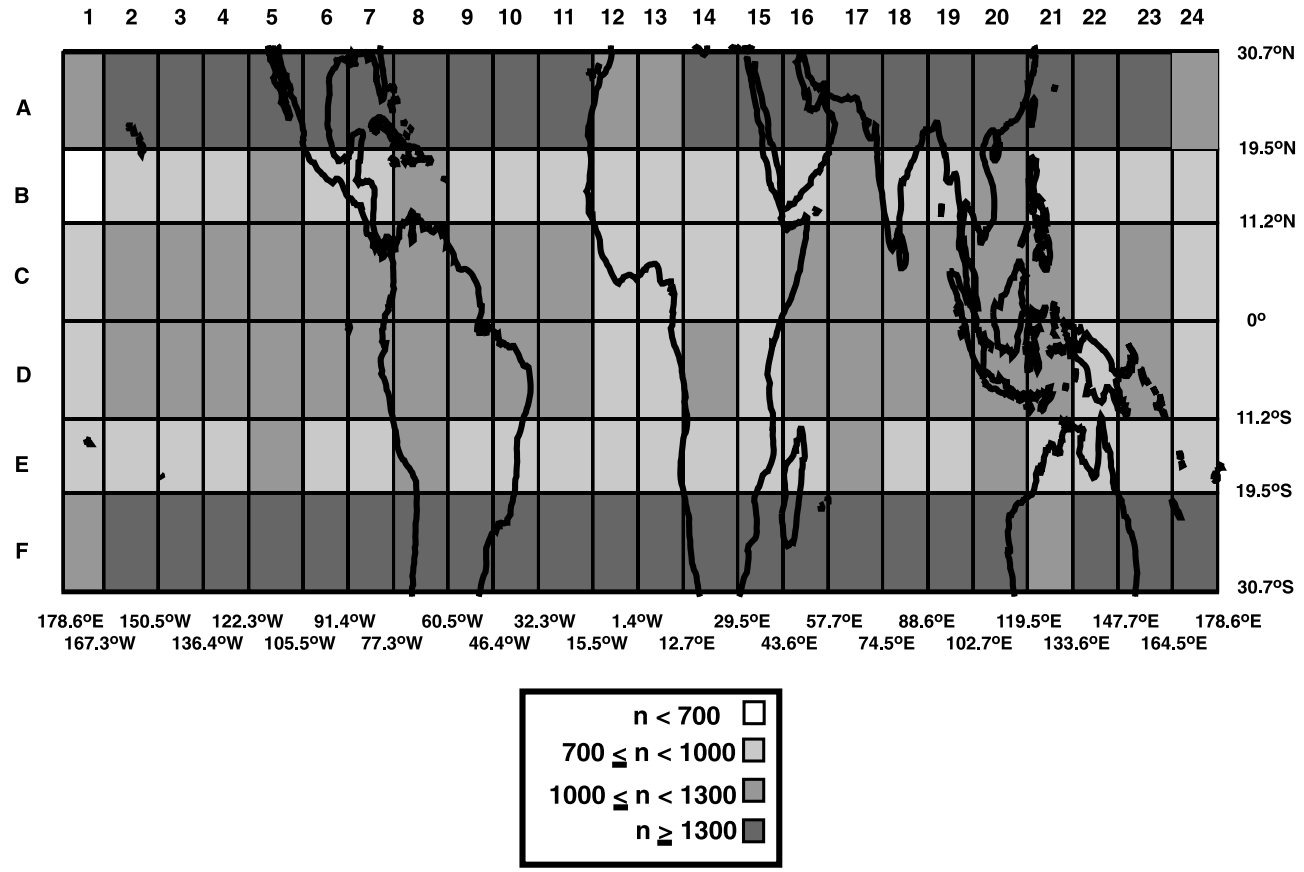


**Figure 2.** Number of samples by the TRMM satellite of the diurnal cycle of precipitation for the 144 regions used in the comparison. The period spans 44 months, from January 1998 through August 2001.

ocean buoys, submitted to Journal of Climate, 2004]. According to *Negri and Bell* [2002] for estimation of the diurnal cycle from TRMM, sampling errors in hourly rain rates, averaged over 36 months and boxes of size $5^\circ \times 5^\circ$ range from 15 to 48% for the PR and from 13 to 34% for the TMI. Because the 3G68 combination product uses both the TMI and PR data, the sampling errors should be similar to those for the TMI. However, the boxes we are using for comparison are much larger than $5^\circ \times 5^\circ$ (about 6 times larger) and thus include more samples. Therefore we expect the sampling errors to be smaller.

### 2.2. GCM Simulations

[6] CCM3 is a three-dimensional global spectral model (see *Kiehl et al.* [1998] for a complete description). For this study, simulations are carried out at T42 horizontal resolution (approximately $2.8^\circ$ latitude $\times$ $2.8^\circ$ longitude) with 18 vertical levels. There is a rigid lid at 2.9 mbar pressure. The model uses a hybrid terrain-following vertical coordinate with sigma coordinates at lower levels that transition to pure pressure coordinates at upper levels. Physical tendency parameterizations include those for clouds [*Slingo*, 1987, 1989; *Ebert and Curry*, 1992; *Cess*, 1985; *Liou*, 1992], radiative fluxes [*Ramanathan*, 1976; *Ramanathan and Downey*, 1986], surface fluxes [*Holtslag and Boville*, 1993], boundary layer height [*Vogelzang and Holtslag*, 1996], and gravity wave drag [*McFarlane*, 1987; *Lindzen*, 1981]. Adjustment physics consists of a convective parameterization following *Zhang et al.* [1998], *Zhang and McFarlane* [1995], and *Hack* [1994], large-scale stable condensation, and dry convective adjustment. One of the inputs for the model is a monthly mean sea surface temperature boundary condition. For this study, we used sea surface temperatures provided to us by the Program for Climate Model Diagnosis and Intercomparison (PCMDI) at Lawrence Livermore National Laboratory [*Taylor et al.*, 2000]. During a model simulation, these monthly mean sea surface temperatures are interpolated to daily values. However, they are not interpolated to hourly values. Thus there is no diurnal cycle of SST in the model. Additionally, the model requires a time-variant ozone mixing ratio boundary data set, and an initial conditions data set that includes initial values of prognostic variables [*Kiehl et al.*, 1996].

[7] Climate models may exhibit considerable internal variability or noise, partly because of fluctuations on synoptic timescales. A single model simulation of an interannual climate event or a climate forecast is can be inadequate for the accurate evaluation of a model's performance [*Chervin*, 1980a, 1980b, 1981; *Barnett*, 1995]. This finding is also valid for CCM3 [*Collier et al.*, 2004]. To distinguish the model's response to natural variations in the SST boundary condition (external variability) from its response to its own internal variability, it is helpful to look at statistics from an ensemble of simulations. Therefore, for this project, we carried out eight separate CCM3 simulations, each forced by exactly the same sea surface temperature boundary condition and differing only in their initial conditions. While the sensitivity of extended range forecast

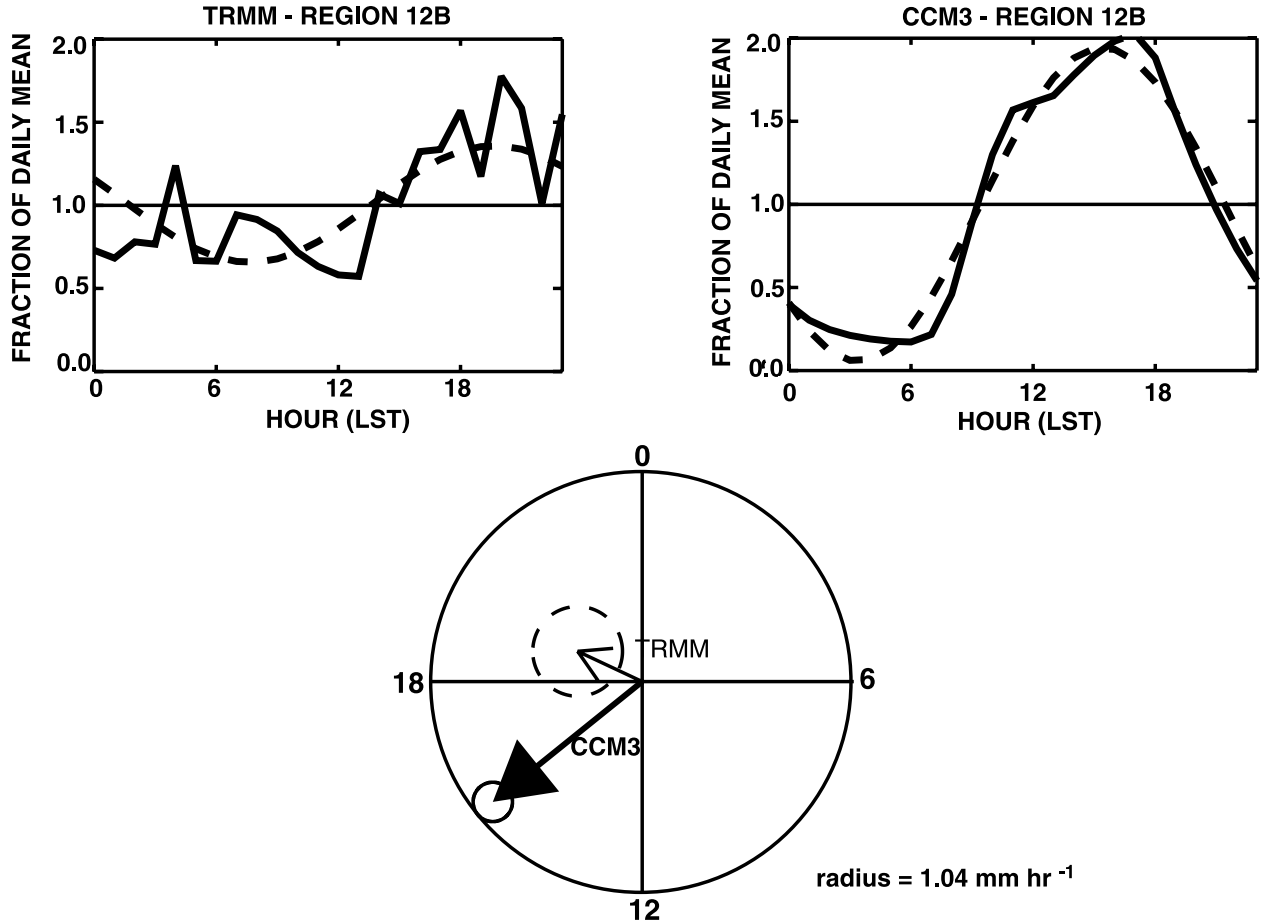


**Figure 3.** (top left) TRMM and (top right) CCM3 climatological mean hourly precipitation as a fraction of daily mean (solid) and diurnal harmonic fit (dashed) for region 12B. (bottom) Phases and amplitudes of the diurnal cycles represented by arrows (CCM3, heavy; TRMM, light) and uncertainty circles (CCM3, solid; TRMM, dashed). A circle which surrounds the arrow's origin indicates that the diurnal harmonic fit is not significant at the 5% level. For clarity, the arrows and associated uncertainty circles have been scaled by a common scale factor.

models to initial conditions is quite significant [*Lorenz*, 1963; *Tracton and Kalnay*, 1993], the actual initial conditions are largely irrelevant to climate forecasts [*Barnett*, 1995], since a climate simulation "forgets" its initial conditions after some limit of deterministic predictability. Therefore, to generate our ensemble, we modified initial conditions among the members by adding random perturbations to the temperature field of a 4-month spin-up run (1 September 1996 to 1 January 1997). The actual perturbation is an exponential function of altitude. By the beginning of the TRMM observing period, in late November of 1997, the realizations have decorrelated from each other and can be treated as statistically independent. Intermember correlations are never identically zero since the observed sea surface temperature field, common to all the members, exerts a common forcing.

[8] The precipitation rates of each simulation, both convective and large scale, are saved as hourly averages. Because the simulations were conducted with 20-min time steps, each hourly average is the average of three time steps. Unless otherwise stated, CCM3 climatological hourly means shown here are ensemble climatological hourly means, and all TRMM results are climatological hourly means averaged onto the CCM3 grid. However, since the sampling errors associated with TRMM are too large on this grid, both data sets are spatially averaged over much larger regions, as shown in Figure 1. A side effect of this design is that some regions encompass both land and ocean. The diurnal variation of precipitation likely is not spatially homogeneous in such a region, a point which must be considered when making conclusions about the model's performance here.

[9] Figure 2 shows how many times the diurnal cycle is sampled by TRMM within each of the regions. Note that there is a maximum number of observations in the northernmost and southernmost rows of regions. These regions are near the highest latitudes sampled by the TRMM satellite. At these latitudes, the satellite orbit is nearly parallel to the latitude lines, so more samples are collected than at lower latitudes.

### 2.3. Harmonic Analysis

[10] The phases and amplitudes of the diurnal cycles, as simulated by CCM3 and as observed by TRMM, are compared on a regional basis as follows. We compute the regional mean precipitation rate at hour $h$ of day $d$, $\overline{r(h,d)}$,

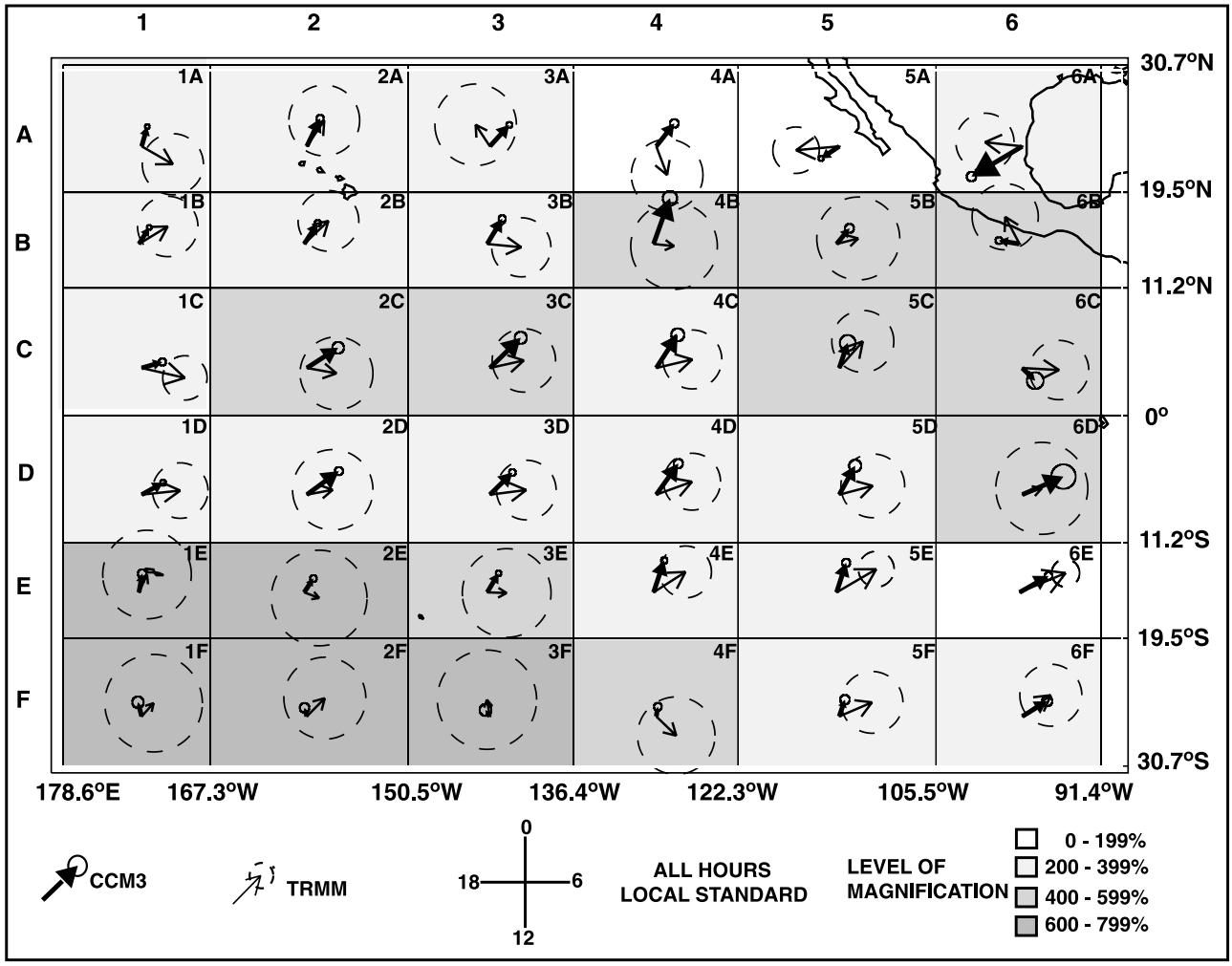


**Figure 4.** Phase of the climatological mean diurnal cycle for regions between the International Date Line and 90°W (CCM3, heavy arrow; TRMM, light arrow), with associated circles of uncertainty. Note that for visibility some of the arrows and associated uncertainty circles have been magnified by a scale factor specific to the region. Thus amplitudes should not be compared between regions.

by averaging over all 2.8° × 2.8° grid boxes $i = 1, \ldots, S$ within the region:

$$\overline{r(h,d)} = \sum_{i=1}^{S} w(h,d)_i r(h,d)_i, \tag{1}$$

where

$$w(h,d)_i = \begin{cases} 1/S & \text{for CCM3} \\ \dfrac{\alpha(h,d)_i}{\sum_{i'=1}^{S} \alpha(h,d)_{i'}} & \text{for TRMM,} \end{cases}$$

such that $\alpha(h, d)_i$ is the fractional area observed by TRMM in grid box $i$ at time $(h, d)$. Next, we compute the "climatological mean" regional mean precipitation rate at hour $h$, $R(h)$, by averaging the regional mean at this hour over all days in the comparison period ($d = 1, \ldots, D = 1338$) using the time analogue of equation (1):

$$R(h) = \sum_{d=1}^{D} W(h,d)\overline{r(h,d)}, \tag{2}$$

where

$$W(h,d) = \begin{cases} 1/D & \text{for CCM3} \\ \dfrac{A(h,d)}{\sum_{d'=1}^{D} A(h,d')} & \text{for TRMM precipitation rates,} \end{cases}$$

such that $A(h, d) = \sum_{i=1}^{S} \alpha(h, d)_i$. The climatological mean regional mean hourly precipitation rates $R(h)$, $h = 0.5, 1.5, \ldots, 23.5$, then are fit to the following model:

$$f(h) = a\cos\frac{2\pi k}{N}h + b\sin\frac{2\pi k}{N}h + c, \tag{3}$$

such that

$$R(h) = f(h) + \delta(h), \tag{4}$$

where $N = 24$, $k = N/24$ for the 24-hour (diurnal) harmonic, and $\delta(h)$ is a residual such that $E[\delta(h)] = 0$, $E[\delta(h)^2] = \sigma^2$, and $E[\delta(h)\delta(h')] = 0$, $h \neq h'$. Parameters $a$, $b$, and $c$ are determined by linear least squares regression and are equivalent to those obtained by fitting the regional means $\overline{r(h,d)}$, to equation (3) with $N = 24D$ and $k = D$ for all $h =$

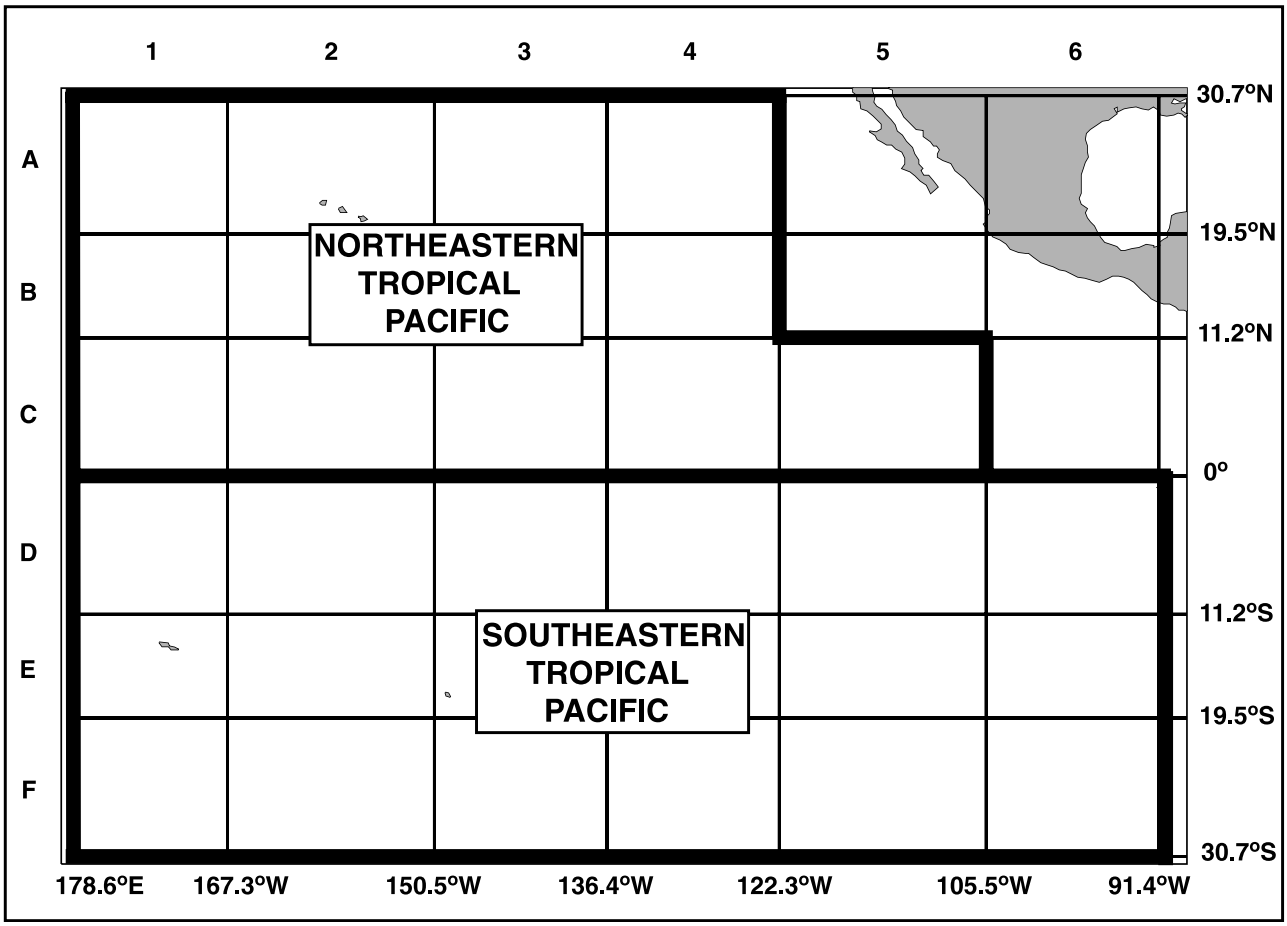


**Figure 5.** Map showing the boundaries of the zones between the International Date Line and 90°W over which CCM3 and TRMM hourly precipitation rates were averaged for comparison.

0.5, . . ., 23.5 and $d = 1,\ldots, D = 1338$. Note that we use a weighted linear least squares regression for the TRMM means, where the weight at each hour $h$ is proportional to the area of the region observed at $h$ totaled over all days in the 44-month comparison period.

[11] Alternately, equation (3) can be expressed as

$$f(h) = A\cos\left(\frac{2\pi k}{N}h - \phi\right) + c, \tag{5}$$

where $A = \sqrt{a^2 + b^2}$ and $\phi = \arctan(b/a)$, representing the amplitude and phase of the diurnal cycle respectively. The test to verify the least squares estimates of $A$ and $\phi$ yields the following condition on the underlying least squares estimates of parameters $a$ and $b$:

$$(\hat{a} - a)^2 + \left(\hat{b} - b\right)^2 \leq \frac{4s^2}{N} F_{2;N-3}(\epsilon), \tag{6}$$

where $s^2$ is the least squares estimate of $\sigma^2$ and $F_{2;\,N-3}$ is the $(1 - \epsilon)$ cutoff value of the $F$ probability distribution function with 2 and (24(samples) − 3(coefficients) =) 21 degrees of freedom. The confidence region is then the circumference and interior of the circle with center $(a, b)$ and radius $\sqrt{4s^2F_{2,21}(\epsilon)/24}$. It is important to note that this test assumes that the data we fit to equation (3) are independent and that the resulting residuals of the fit are normally distributed. As for the first assumption, averaging the output over the ensemble members, which are effectively independent, gives effectively uncorrelated rain rates. While the second assumption may not be valid in the strictest sense, a $(1 - \epsilon)$% confidence circle still provides a useful metric for this comparison, as its size is directly proportional to the sum of the squared differences ($s^2$) between the fit and the data. For our purposes we set $\epsilon = 0.05$ and use the resulting circle to represent the uncertainty associated with fitting $R(h)$ to $f(h)$. Contained within each uncertainty circle are points $(A, \phi)$ which may be assumed to represent $f(h)$ within a constant level of uncertainty. Assuming the data are independent and that the residuals are normally distributed, all points $(A, \phi)$ within the circle would pass the goodness-of-fit test at the 95% level. For further details on the statistical test, we refer the reader to *Anderson* [1978].

[12] Figure 3 illustrates the application of the above method to a region in western Africa (region 12B). The top panel of the Figure 3 shows a least squares fit to the climatological mean regional mean diurnal cycle as observed by TRMM and as simulated by CCM3. In the bottom panel, the phases and amplitudes of the harmonic fits to

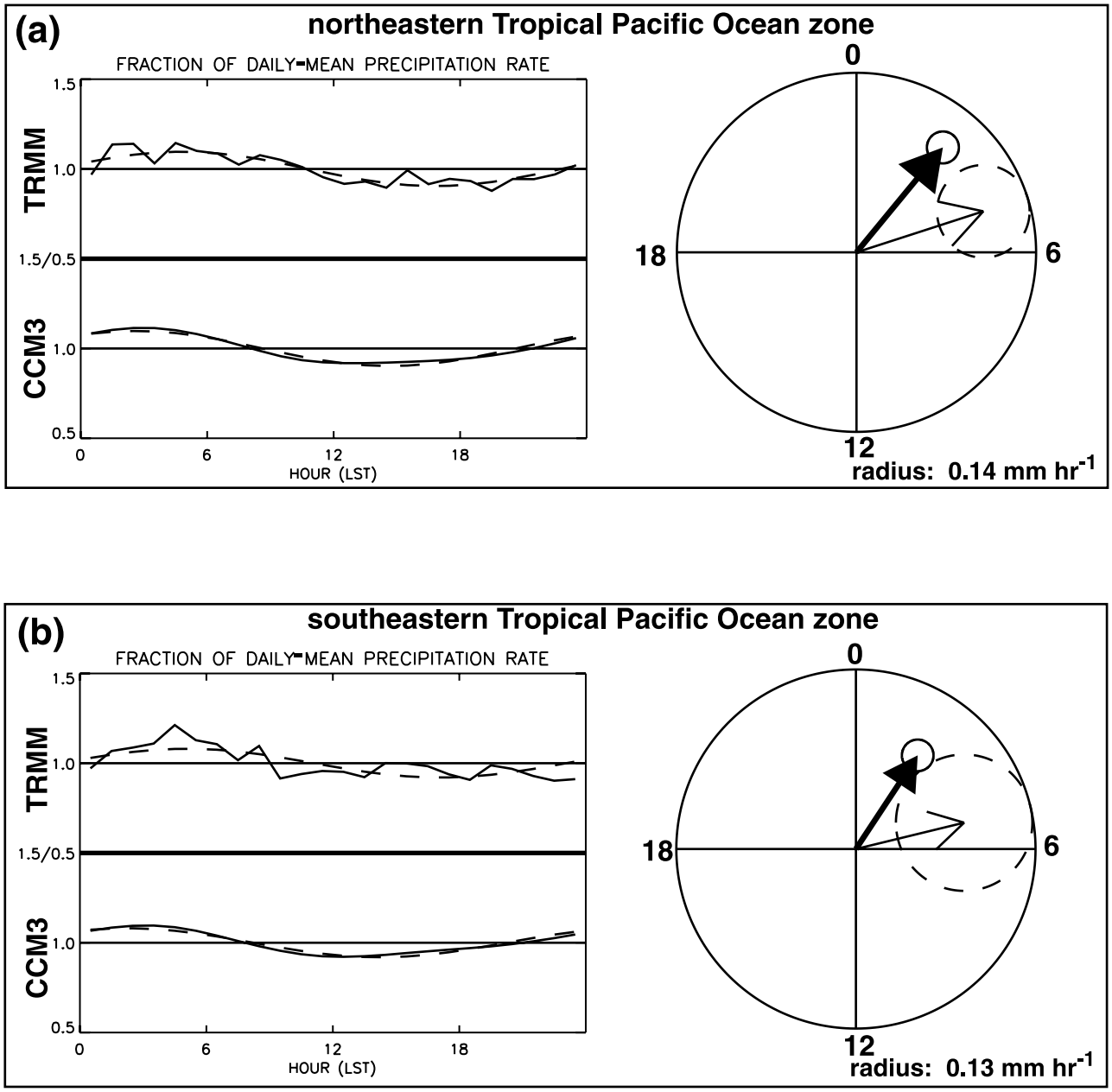


**Figure 6.** The TRMM and CCM3 climatological mean hourly precipitation for the (a) northeastern tropical Pacific Ocean zone and (b) southeastern Pacific Ocean zone. (left) Cimatological mean hourly precipitation is expressed as a fraction of daily mean (solid) with its diurnal harmonic fit (dashed). (right) Phases and amplitudes of the diurnal harmonic fits are expressed in arrow–uncertainty circle format (CCM3, heavy arrow and solid circle; TRMM, light arrow and dashed circle).

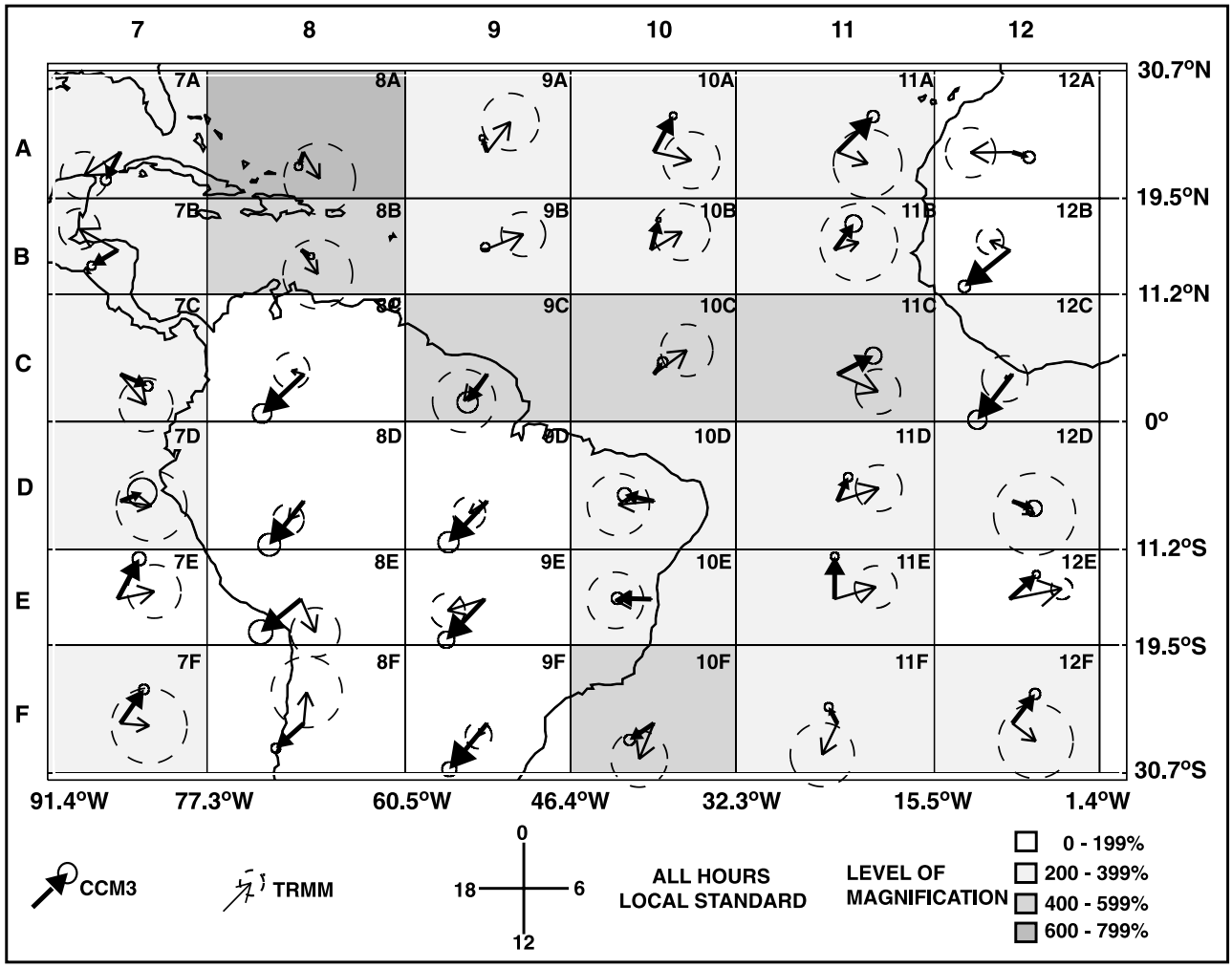


**Figure 7.** Same as in Figure 4 except for regions between 90°W and the prime meridian.

the diurnal cycles are represented by arrows and uncertainty circles as cast into the standard 24-hour clock. For both the CCM3 and TRMM results, the uncertainty circle gives an estimate of the sampling error associated with fitting the diurnal cycle. Owing to the large sample size, the CCM3 sampling errors are generally small. Because the TRMM sample sizes are much smaller, sampling errors can be substantial. In the following discussion, results will be presented in the above arrow-circle format. In general, differences in phase and magnitude between the model output and the satellite data are measured based on distances between the arrowheads, which represent the most likely values of amplitude and phase.

## 3. Results

### 3.1. Western Tropical Western Hemisphere (International Date Line to 90°W)

[13] Figure 4 shows the phases and relative amplitudes of the diurnal harmonic fits to the climatological mean regional mean diurnal cycles of precipitation for all regions between the International Date Line and 90°W. Each arrow-circle diagram is plotted on top of its region on the map, where north indicates hour 0, east indicates hour 6, south indicates hour 12, west indicates hour 18, and all hours in local standard time. As in Figure 3, the uncertainty circles provide bounds on a range of amplitudes and phases that fit the diurnal harmonic, in as much as it is an appropriate model. If the uncertainty circle surrounds the origin of its arrow, an amplitude of zero is possible, indicating that the precipitation over the associated region demonstrates no significant diurnal signal. If the CCM3 circle overlaps the TRMM circle, and if neither circle surrounds the origin of its arrow, the phase and magnitude differences between the diurnal cycles lie within the measured uncertainty of the fit, and thus are not significantly different. It is important to note that for each region, the lengths of both arrows and the radii of the uncertainty circles have been magnified (or demagnified) by a scale factor common to the region. The scaling was done so that the diagrams from all regions could be seen, since the diurnal cycles over some regions are much stronger than those over others. As a result, the amplitudes of the diurnal cycles cannot be compared between regions. The level of magnification is indicated by background shading in the region (lightest shading represents a downscaling (less than 100%) or slight upscaling (between 100 and 200%) while darkest shading represents a large upscaling (greater or equal to 600%)). The largest magnification is done where diurnal signals are weak.

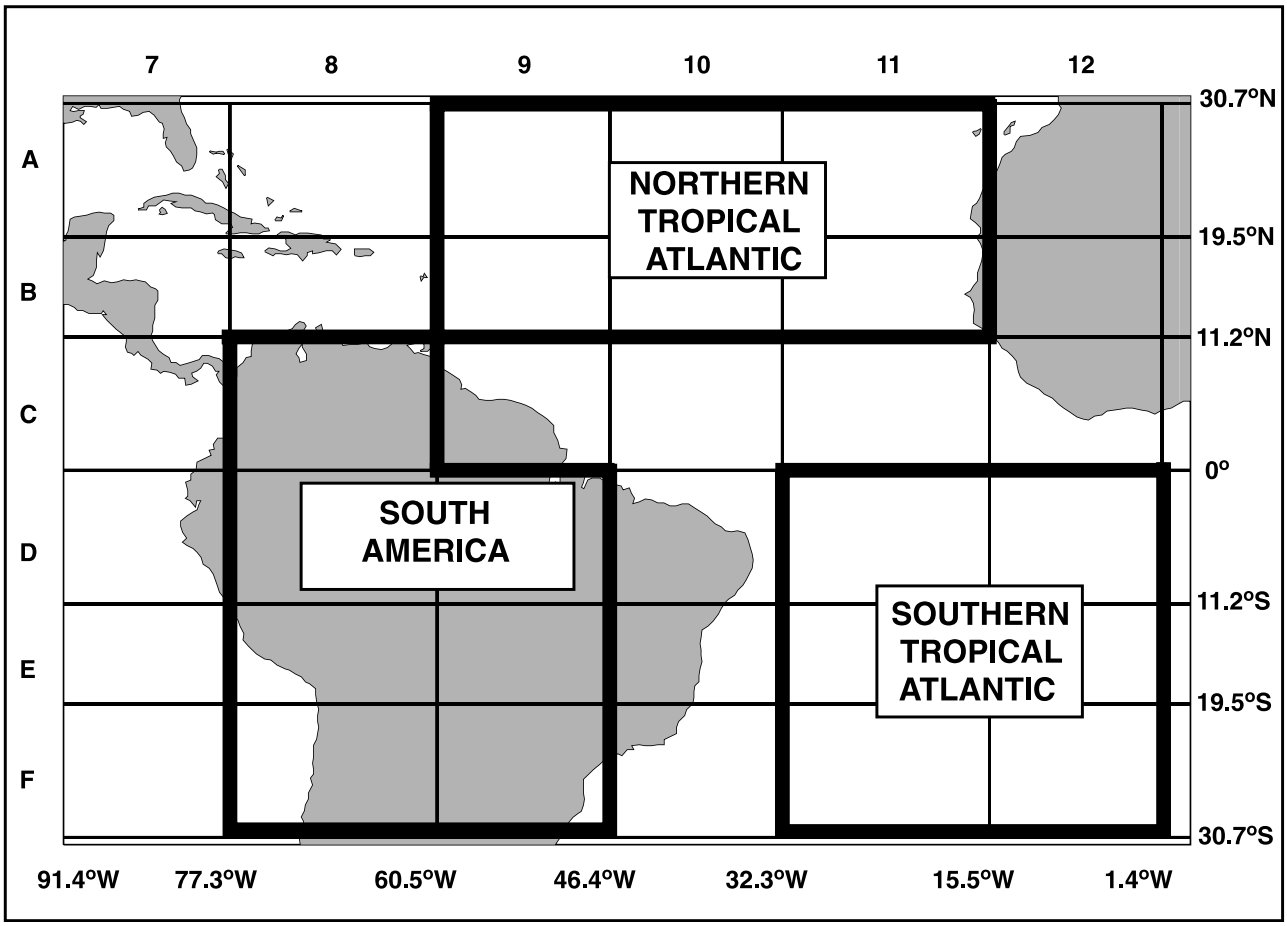


**Figure 8.** Map showing the boundaries of the zones between 90°W and the prime meridian over which CCM3 and TRMM hourly precipitation rates were averaged for comparison.

[14] For most of these regions, the model simulates diurnal variations of precipitation that are statistically significant. However, in some regions, a great amount of magnification is needed in order to see them (i.e., the southwestern regions 1E, 2E, 1F, and 2F). In most regions, there is very little uncertainty with the diurnal harmonic fit to the CCM3 output, both in amplitude and in phase. The model simulates an early morning peak in the day's precipitation in nearly all regions, save regions close to Central America (5A, 6A, 6B, and 6C). These are coastal regions, where there may be competing influences from differing diurnal cycles over land and ocean. Region 6A is primarily continental. For most regions, the TRMM uncertainty circles surround the origins of its arrows. Thus, if the statistical assumptions stated above are approximately valid, then for most regions, the TRMM results are not statistically significant at the 5% level. However, the TRMM amplitudes are generally consistent with those of the model, while the TRMM phases are consistently several hours later than those of the model. There are a few exceptions where phases compare quite well. These are found near the western and eastern boundaries of the zone (in 2A, 2B, and 1E and 6D, 6E, and 6F, respectively). Amplitudes do not agree quite as well in the eastern boxes (6D, 6E, and 6F), with CCM3 about twice as large as TRMM in 6D and about 25–50% to small in 6E and 6F. To make conclusions about model-satellite differences over the remaining area in this sector, we average the TRMM data over even larger regions, or "zones," as seen in Figure 5, and recompute our least squares fit parameters.

[15] The results of the least squares fits to the climatological mean zone mean hourly precipitation rates for the northeastern tropical Pacific zone are shown in Figure 6a. Averaging the TRMM data over this large zone significantly reduces the size of the TRMM uncertainty circle, as seen in the corresponding individual regions. Both the diurnal harmonics in CCM3 and in TRMM are of about the same magnitude, roughly 10–15% of the daily mean and thus are relatively weak over this oceanic zone. Both exhibit early morning peaks in precipitation, though that for CCM3 precedes that of TRMM by approximately 2 hours. Over the southeastern tropical Pacific Ocean zone to the south (Figure 6b), the amplitudes of the diurnal harmonics are comparable (about 10–15% of the daily mean), but the phases differ by 3 hours, with CCM3 leading TRMM, although the uncertainty circles are fairly large.

### 3.2. Eastern Tropical Western Hemisphere (90°W to Prime Meridian)

[16] Figure 7 shows the phases and magnitudes of the diurnal harmonic fits to the diurnal cycles in regions between 90°W and the prime meridian. This sector of the tropics provides a nice sample of the diurnal cycle over both ocean and land. We begin over South America, where the

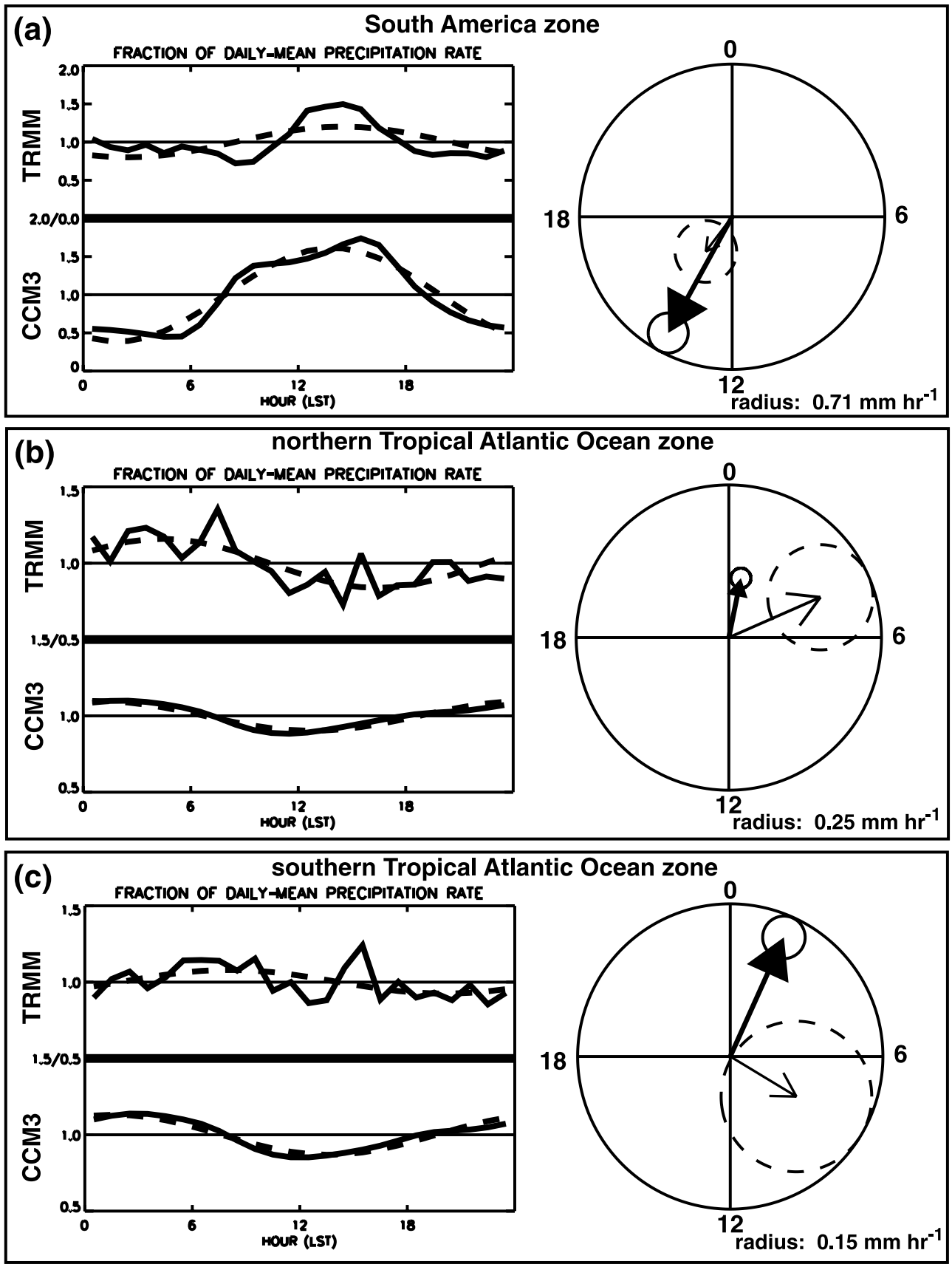


**Figure 9.** Same as in Figure 6 except for the (a) South American zone, (b) northern tropical Atlantic Ocean zone, and (c) southern tropical Atlantic Ocean zone.

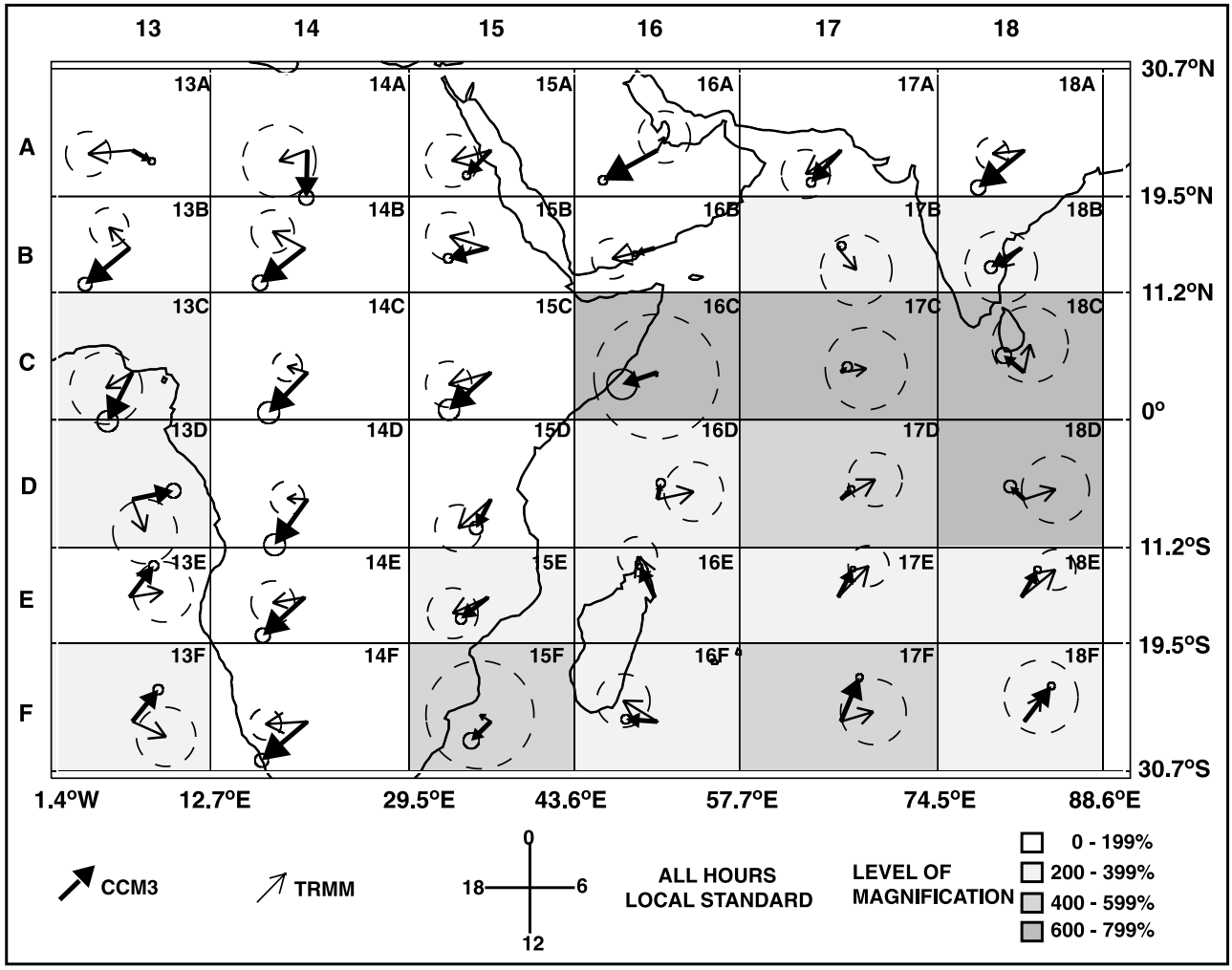


**Figure 10.** Same as in Figure 4 except for regions between the prime meridian and 90°E.

comparison between CCM3 and TRMM is relatively straightforward: uncertainty circles are not too large in these regions. CCM3 demonstrates peaks in the diurnal harmonic during the early to mid-afternoon hours (evening in the eastern coastal regions, where the diurnal cycle of the oceans may be mixed in). Over these regions, the model is in fair agreement with TRMM in terms of the timing of the peak. Such an agreement is particularly evident in regions 8D, 9D, and 9F, and not so much in region 9E, where the model's peak precedes that of the observations by nearly 2 hours. Despite its reasonable success with timing over for most regions of South America, the model overestimates the amplitude of the diurnal variation, relative to the observations. For example, in region 9F, the model's amplitude is about 4 times as large as TRMM's. Again, region 9E looks to be the exception. Though the phases do not agree as well in this region, the magnitudes of diurnal variation are comparable.

[17] The model-satellite comparison is relatively straightforward over western Africa (regions 12A and 12B). Here the uncertainties associated with the TRMM fits to the diurnal harmonics are comparatively small. In region 12A, the model and satellite differ substantially in phase and in amplitude, with the model preceding TRMM by nearly 11 hours in its diurnal harmonic peak, exhibiting the maximum precipitation during the morning instead of during the afternoon. In addition, the amplitude of the model's peak is at least 50% smaller. By contrast, in region 12B, the model's diurnal harmonic amplitude is at least twice that of TRMM and the peak in its harmonic is only about 4 hours earlier.

[18] In regions of the northern tropical Atlantic (rows A and B, columns 9 and 10), there is much uncertainty in the TRMM fits, and averaging more of the TRMM data together may support more conclusive comparisons (see below). In the southern tropical Atlantic, south of the Equator and east of South America, (rows D, E, and F, columns 11 and 12), there are similarly large uncertainties (regions 11F, 12D and 12F especially). The exceptions lie in regions 11D, 11E, and 12E. The model's peak in the diurnal harmonic is seen to precede that of the observations by about 2 hours in 12E, by 3 hours in 11D, and by nearly 5 hours in 11E. As we do for the sector to the west, we average the model output and satellite data in this sector over larger zones, as depicted in Figure 8, and compute the least squares fits for analysis on larger scales.

[19] Averaging the model output and satellite data over South American regions (Figure 9a) confirms earlier find-

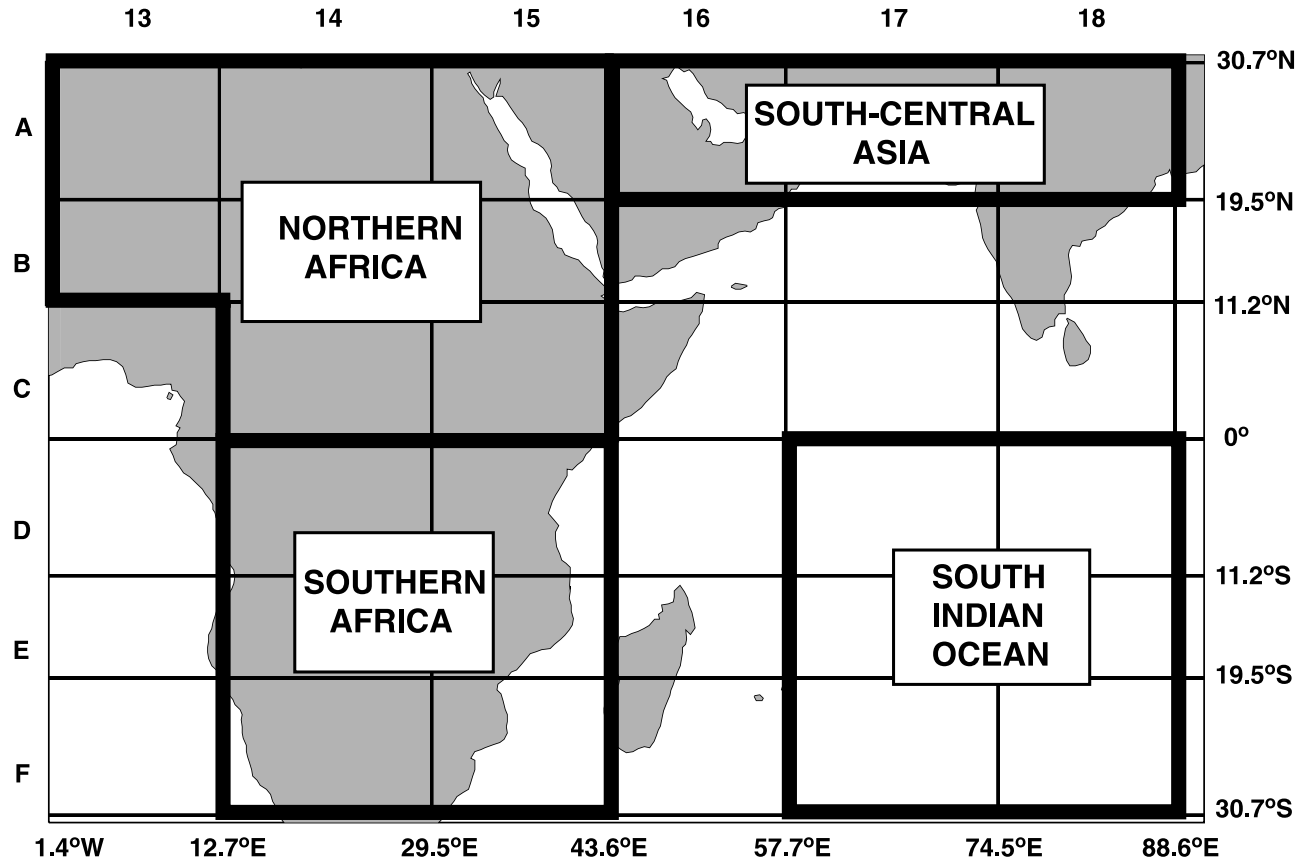


**Figure 11.** Map showing the boundaries of the zones between the prime meridian and 90°E over which CCM3 and TRMM hourly precipitation rates were averaged for comparison.

ings on the regional scale. The amplitude of the CCM3 diurnal harmonic is about 3 times the amplitude of the TRMM diurnal cycle, though the phases of the diurnal harmonics are reasonably collocated in time, in mid-afternoon. For the northern tropical Atlantic zone (Figure 9b), averaging does little to reduce the size of the uncertainty circle surrounding the TRMM arrow. However, it is clear that both the model and satellite show diurnal harmonic peaks in the early morning hours (between midnight and dawn), with the CCM3 peak coming about 3 to 4 hours before the TRMM peak. Over the southern tropical Atlantic zone (Figure 9c), the TRMM uncertainty circle is large enough to indicate that there is no significant diurnal cycle present in the data. The large uncertainty might result from averaging over too many regions here, lumping together regions whose fits to the diurnal harmonic differ widely.

### 3.3. Western Tropical Eastern Hemisphere (Prime Meridian to 90°E)

[20] Figure 10 shows the phases and amplitudes of the fits of the CCM3 and TRMM precipitation rates to the diurnal harmonic for regions between the prime meridian and 90°E. Much of this sector of the tropics is land and includes the majority of the African continent. With a few exceptions, over much of interior Africa (column 14 and regions 13A and 13B), the CCM3 diurnal harmonic peaks relatively strongly in mid-afternoon, though it peaks slightly earlier in the Congo regions of 14C and 14D. In most regions, the model's peak precedes that of TRMM by 2 to 4 hours, with the largest phase differences generally located north of the Equator in regions 13B, 14B, and 14C. South of the Equator, there is slightly better agreement between the simulation and the observations. While regions 14D and 14E differ substantially in amplitude such that the uncertainty circles do not overlap, the range of phases do. As for the amplitudes, CCM3 and TRMM agree best in regions 13B, 14B, 14E, and 14F, given the size of the TRMM uncertainty circle. Regions 13A and 14A in the Sahara Desert are the significant outliers in interior Africa. In region 13A, as in region 12A (see Figure 7) to the west, CCM3 shows a peak in the diurnal harmonic just after dawn. As they do in 12A, the satellite observations fairly certainly indicate a peak in the late afternoon or evening (between one quarter and one half of a cycle after the model). In 14A, the model exhibits a strong peak in its diurnal harmonic near noon, while the TRMM satellite data show no significant diurnal cycle at all or are too sparse for a good fit. In contrast to the inhomogeneities over interior Africa, in eastern Africa (column 15), the model output and satellite data agree rather uniformly. There is overlap in phase and in magnitude in all of these regions save 15F, with peaks in the diurnal harmonics occurring in mid to late afternoon.

[21] Over regions of south Asia, there is good agreement in the phase of the diurnal harmonic in regions 16B and 17A with peaks in middle to late afternoon. The CCM3 amplitude is slightly smaller than that of TRMM in region 16B, but the amplitudes are comparable in 17A. In region 16A, the model

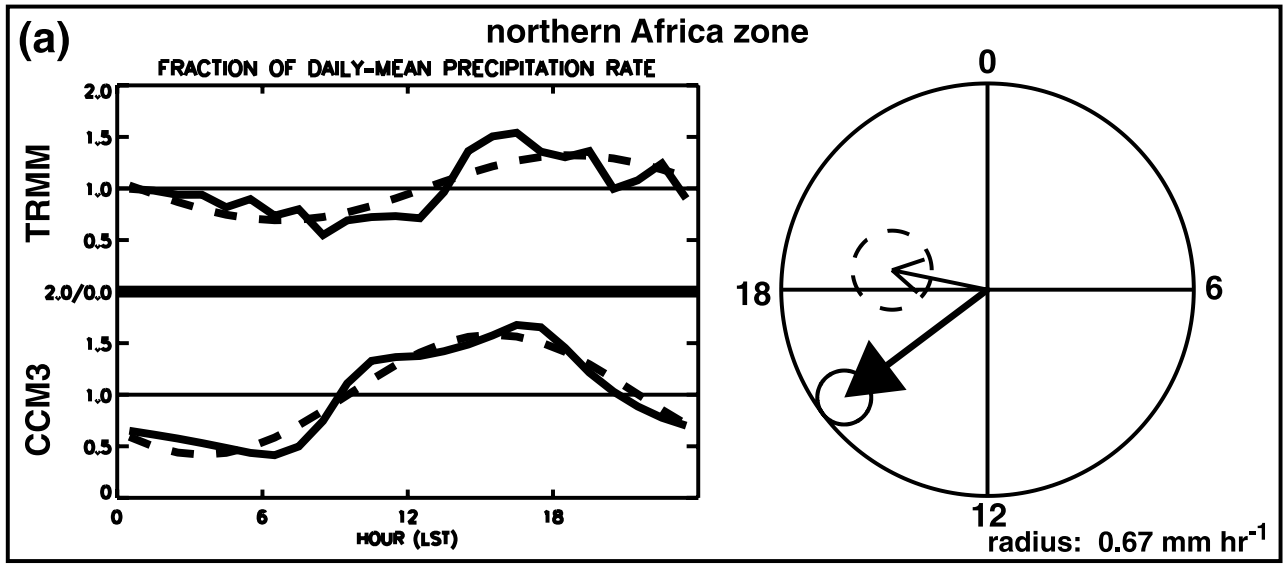


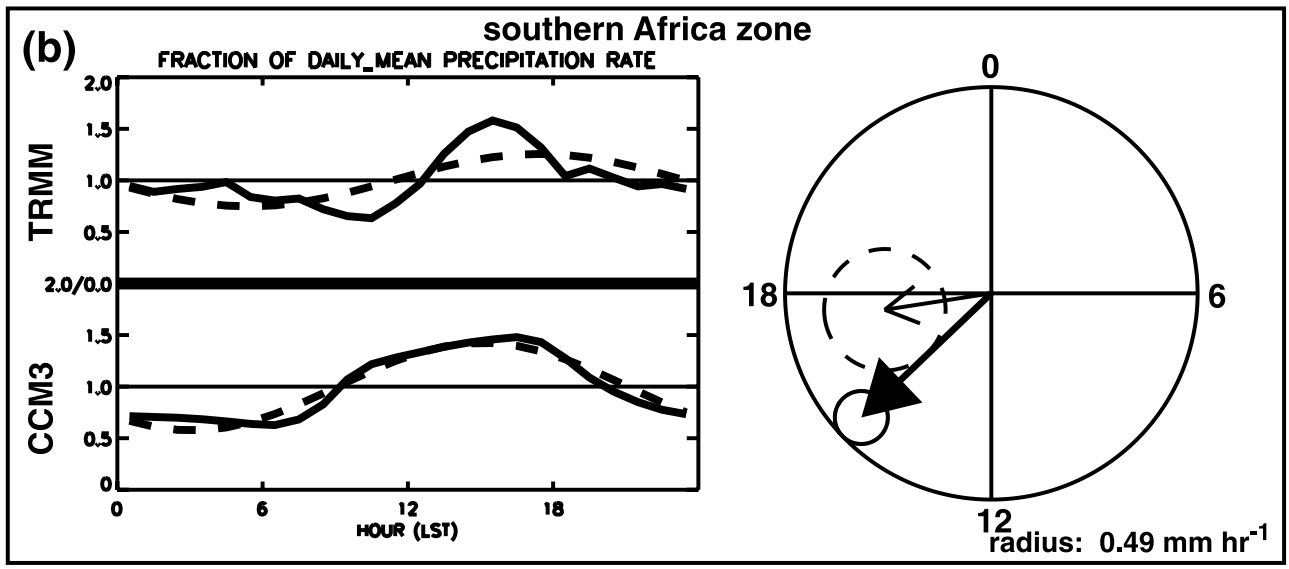


**Figure 12.** Same as in Figure 6 except for the (a) northern Africa zone and (b) southern Africa zone.

produces a robust diurnal signal, which is nonexistent in the TRMM observations. Monthly mean precipitation rates also disagree in the region [*Collier et al.*, 2004]. In regions 17A and 18A, over the Indian subcontinent, the phases are in fairly good agreement, given the magnitude of the uncertainty in the fit of the TRMM data here.

[22] Over the Indian Ocean, it is difficult to make a comparison between the model and the satellite. The uncertainties associated with fitting the TRMM precipitation rates to the diurnal harmonic are quite large here. Where TRMM shows a significant diurnal variation (regions 17E and 18E), the model-satellite differences in phase and amplitude are generally small.

[23] For the longitude sector from the prime meridian to 90°E, we average the output and data over large zones whose boundaries are depicted in Figure 11. Figure 12a shows the diurnal cycles of precipitation for TRMM and CCM3 and their fits to the diurnal harmonics for regions in the northern Africa zone. Over this zone, the CCM3 diurnal cycle is larger than that of TRMM, with the model's peak in the diurnal harmonic occurring about 3 hours earlier than observed. As seen in the regional comparison, the difference certainly is largest over region 13A, in the Saharan Desert. Over southern Africa (Figure 12b, the amplitude of the model's diurnal harmonic is between 50 and 60% of the daily mean, while that of the observations is roughly half. The phases of the diurnal harmonics are in fairly good agreement here, given the size of the TRMM uncertainty circle; however, the phase difference is more apparent in the means plot where

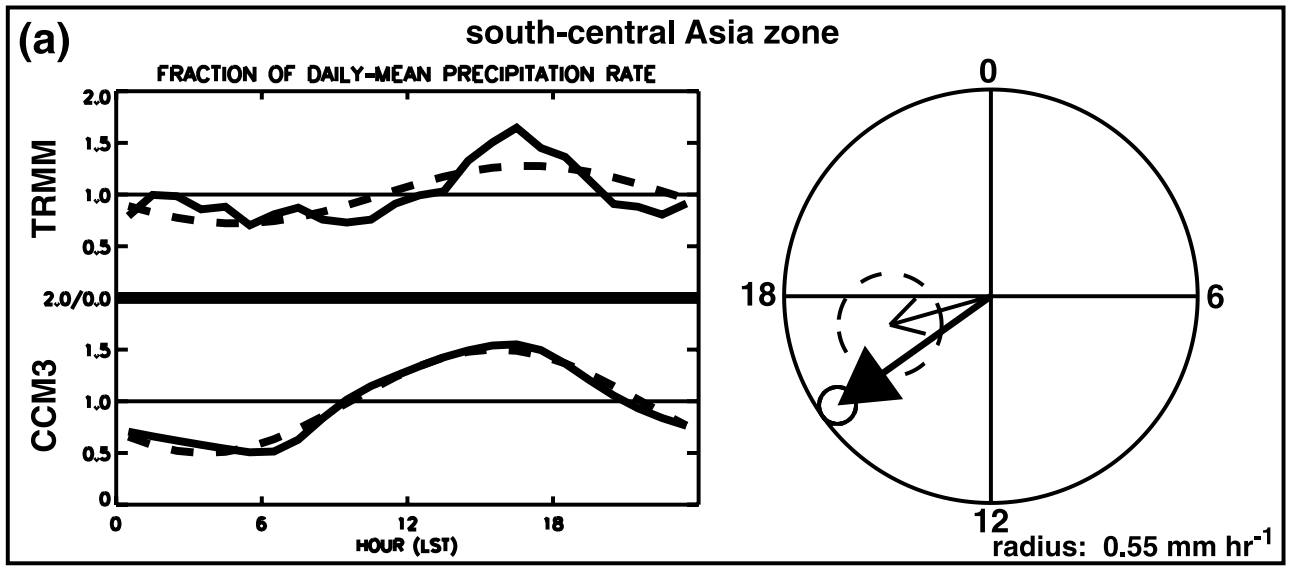


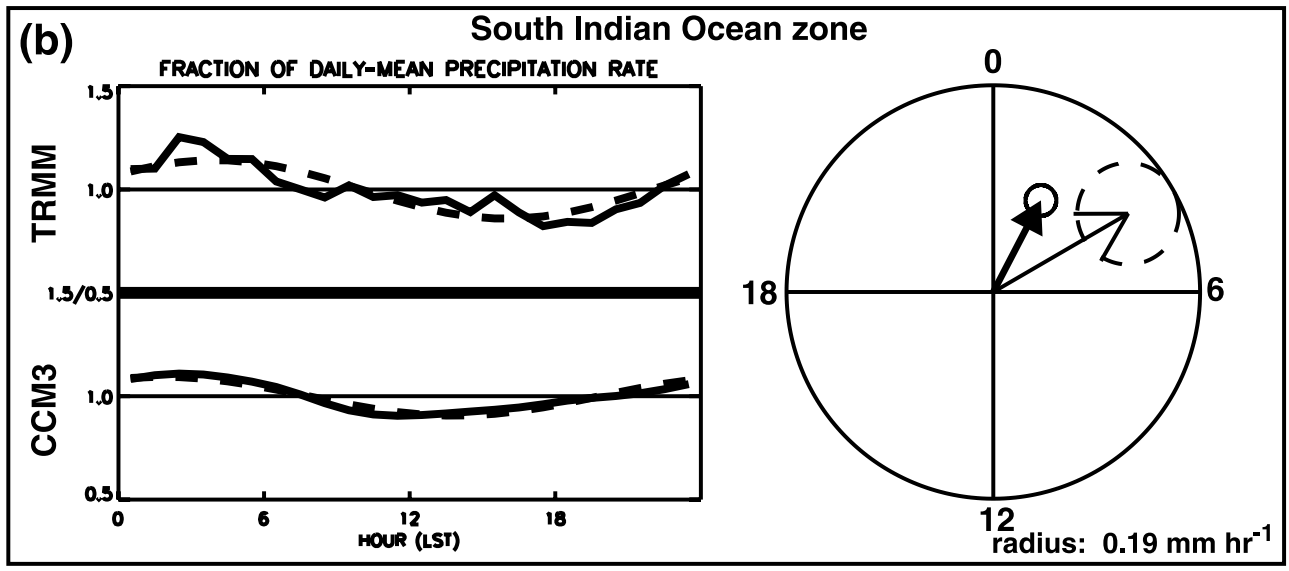


**Figure 13.** Same as in Figure 6 except for the (a) south central Asia zone and (b) South Indian Ocean zone.

CCM3 leads the TRMM observations by 2 to 3 hours. In the south central Asia zone (Figure 13a), the uncertainty circles overlap in phase, with both arrows indicating a peak anywhere from 1400 to approximately 1900. While the model's amplitude appears only 80% larger in the zone mean, it should be noted that the difference is significantly larger over region 16A, the eastern Arabian peninsula, where TRMM indicates little to no regular diurnal variation at all.

[24] Averaging the model output and satellite data over the South Indian Ocean zone (Figure 13b) substantially aids in the comparison of the diurnal cycles. The uncertainty associated with the fit of the TRMM data to the diurnal harmonic is smaller at this large spatial scale. Though the diurnal cycles are quite small over this oceanic zone and require a great amount of magnification to see on the regional scales, it is evident on the zone scale that the simulated diurnal cycle is about half as large as that which is observed. The peak in the model's diurnal harmonic, shortly after midnight, precedes that of the observations by about 2 hours.

### 3.4. Eastern Tropical Eastern Hemisphere (90°E to International Date Line)

[25] Figure 14 shows the phases and amplitudes of the fits of the CCM3 and TRMM precipitation rates to the diurnal

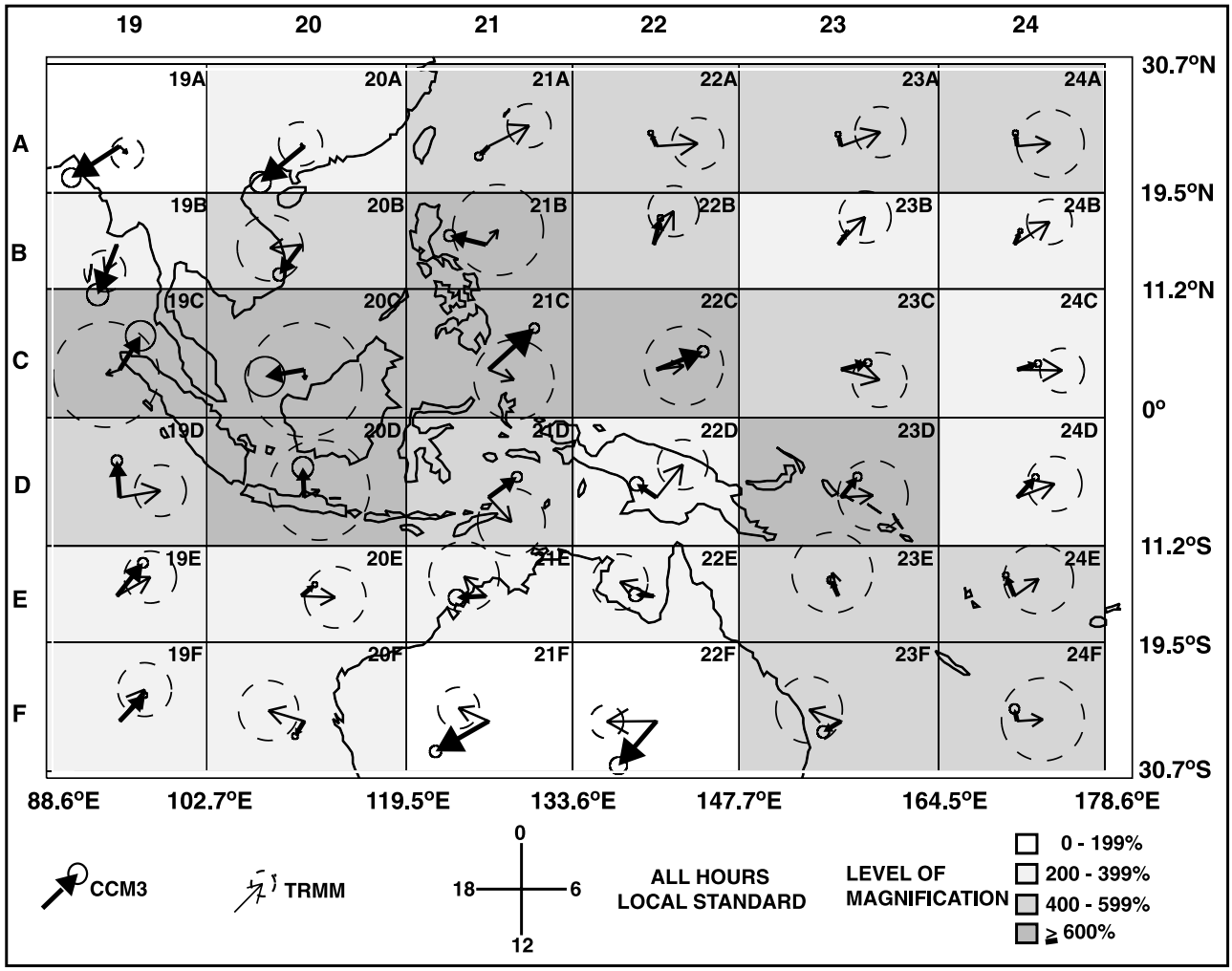


**Figure 14.** Same as in Figure 4 except for regions between 90°E and the International Date Line.

harmonic for regions between 90°E and the International Date Line. For many regions in this sector, large uncertainties in the least squares estimates of the diurnal harmonics makes model-satellite comparisons difficult. There are a few exceptions where comparisons can be made easily. For example, CCM3 and TRMM compare relatively well in both phase and amplitude in region 19B. In contrast, in neighboring regions 19A and 20A, the model simulates a strong diurnal variation, which is not seen in the observations. There are two regions over the Maritime Continent in which CCM3 and TRMM can be compared easily. In region 19D over the eastern equatorial Indian Ocean, the model-simulated diurnal harmonic agrees well with the observed diurnal harmonic in magnitude but leads in its phase by about 6 hours. Similarly, the magnitudes compare well in region 22D over Papua New Guinea, but the model's diurnal harmonic peak precedes that of TRMM by 5 to 6 hours. Farther south, over Australia, model-satellite differences are generally similar, with the model preceding the observations (only slightly in region 21F but by 3 to 4 hours in region 22F). There are model-satellite differences in both phase and magnitude over regions of the northwestern tropical Pacific. CCM3 shows a much weaker diurnal cycle than that which is evident in the TRMM observations here. The peak of the model's diurnal harmonic appears to precede that of TRMM by at least 10 hours in region 21A, by at least 6 hours in 23A, and by at least 4 hours in 22A. The phases agree better in 22B, 23B, 24B, 23C, and 24C to the south.

[26] The boundaries of the zones over which we spatially average the CCM3 output and the TRMM data are shown in Figure 15. The phase and amplitude comparisons for these zones are shown in Figures 16 and 17. For the Southeast Asia zone (Figure 16a), the model simulates a moderately strong diurnal variation of precipitation, approaching 20–30% of the daily mean. Contrast this variation with that observed by TRMM over this zone: observations show little to no diurnal variation at all, which is confirmed by a poor fit to the diurnal harmonic. The fit of the CCM3 output to this harmonic is quite good by comparison and indicates a daily peak in precipitation in mid-afternoon. Thus our averaging over these regions of the tropics indicate that the very regular diurnal variation of precipitation as simulated by the model does not compare well with TRMM observations, which indicate a variation that is much more irregular. To the south, both model and satellite show little to no diurnal cycle of precipitation over the Maritime Continent (Figure 16b), but partly because we average over

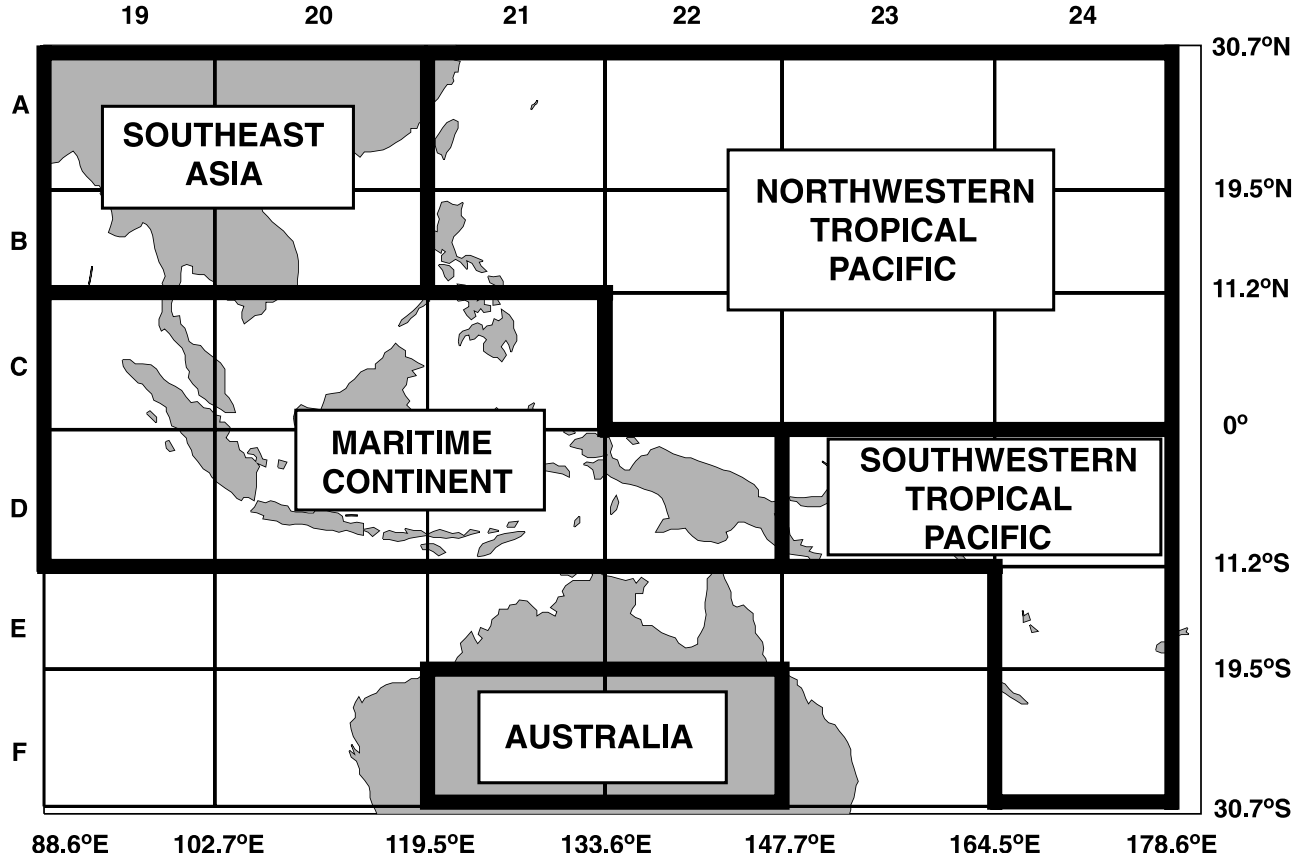


**Figure 15.** Map showing the boundaries of the zones between 90°E and the International Date Line over which CCM3 and TRMM hourly precipitation rates were averaged for comparison.

regions which contain both land and ocean and thus presumably very different diurnal cycles. Certainly, there is a pronounced diurnal signal over the far eastern equatorial Indian Ocean (region 19D) and over Papua New Guinea (region 22D), as seen by TRMM and as simulated by the model. The differences in phase over these regions is noticeable: CCM3 precedes TRMM in the peak of the diurnal harmonic by 1 to 2 hours in region 19D and by 2 to 3 hours in region 22D. Unfortunately, it would be difficult to make comparisons over the other islands in this region because of TRMM's sampling errors. The Australia zone (Figure 16c) is entirely land, and a pronounced diurnal signal is evident in both the model output and the satellite data. Over this zone, the difference is primarily one of phase, as magnitudes agree quite well. The CCM3 output shows an ample peak in the diurnal harmonic in mid-afternoon, at least 5 hours earlier than the daily peak evident in the TRMM data (evening).

[27] Over the ocean zones to the east (Figure 17), the TRMM diurnal signal shows up much better than on the regional scales considered above. Diurnal variations, as simulated by CCM3 and as observed by TRMM are small in these zones of the western tropical Pacific. The CCM3 diurnal variation is smaller than that observed by TRMM over the northwestern tropical Pacific (Figure 17a) but is of comparable magnitude to the south (Figure 17b). Over the northwestern zone, the CCM3 diurnal harmonic leads the TRMM diurnal harmonic in phase by 2 to 3 hours. However in 21A, it leads TRMM by 10 to 11 hours. Over the southwestern zone, the model's diurnal harmonic peak precedes that of the data by 3 to 4 hours.

## 4. Summary and Conclusions

[28] The diurnal variation of precipitation is a much studied quantity. Most observational studies tend to agree that the diurnal cycle is larger over land than over the oceans. In addition, many have found that daily precipitation peaks between noon and midnight over land and between midnight and noon over the oceans. Various physical mechanisms have been hypothesized to explain this difference. It is important that general circulation models correctly simulate the diurnal variations in precipitation, and previous researchers have taken advantage of the observational studies to validate models. The present research compares hourly averaged precipitation rates from an ensemble of eight realizations from the NCAR CCM3 for the 44-month period from January 1998 through August 2001 to observations from the Tropical Rainfall Measuring Mission (TRMM) satellite. Comparisons are made within 15° longitude × 10° latitude boxes and within even larger geographical zones in the tropics. The temporally and spatially averaged hourly precipitation rates from CCM3 and from TRMM are fit to the diurnal harmonic by the method of linear least squares regression, and the phases and the amplitudes of the diurnal harmonics are compared.

[29] The results of this analysis show that, with a few exceptions, over much of the tropical oceans and some of

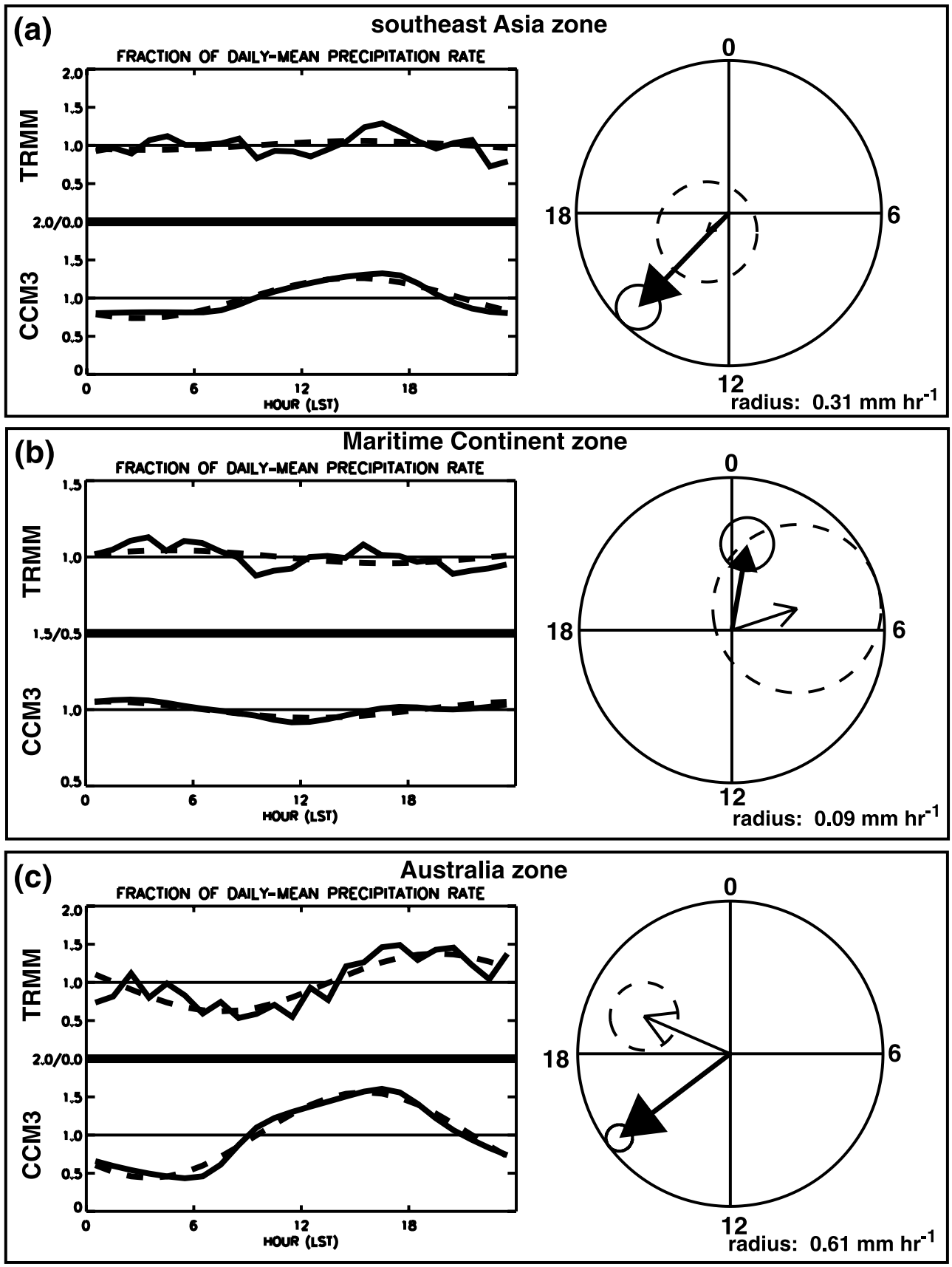


**Figure 16.** Same as in Figure 6 except for the (a) Southeast Asia zone, (b) Maritime Continent zone, and (c) Australia zone.

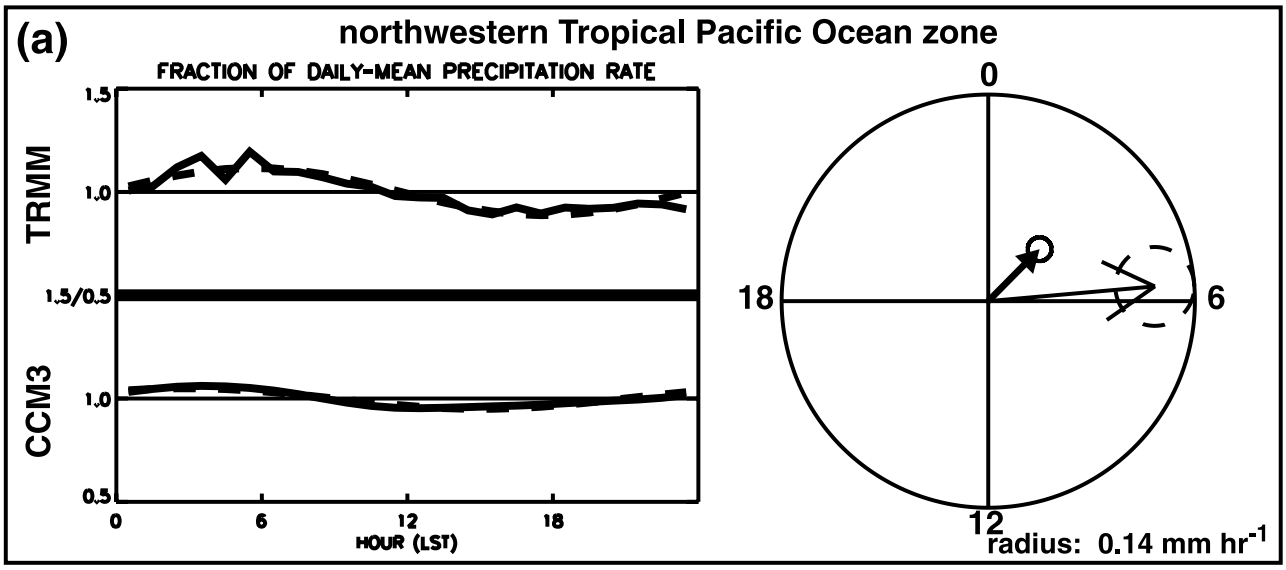


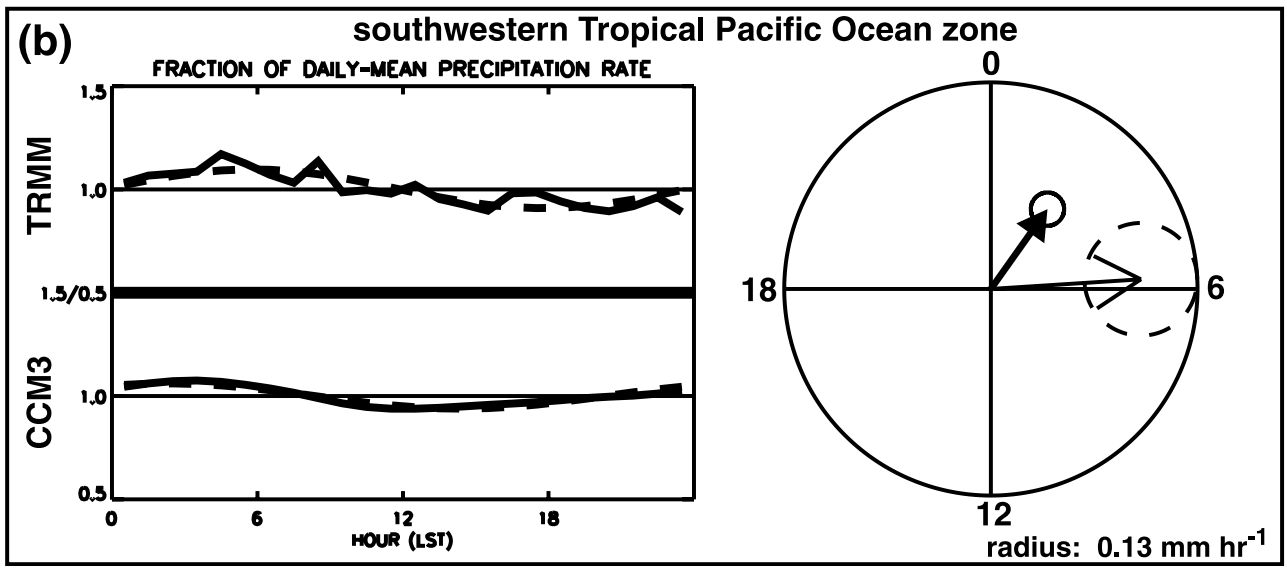


**Figure 17.** Same as in Figure 6 except for the (a) northwestern tropical Pacific Ocean zone and (b) southwestern tropical Pacific Ocean zone.

the tropical land masses, comparisons on the regional scales defined are often quite difficult because of the large amount of uncertainty associated with fitting the TRMM data to a diurnal harmonic. Some of this uncertainty is due to insufficient sampling, while some is due to weak diurnal signals, especially over the ocean. When averaged over the geographical zones, the diurnal variations as observed by TRMM become more recognizable, and more straightforward comparisons can be made. We summarize the results of the comparisons within the geographical zones in Table 1.

[30] We find that, compared to the TRMM satellite data, CCM3 tends to overestimate the amplitude of the diurnal cycle of precipitation over most landmasses considered in this study. The largest biases are found in the simulations over south central Asia, northern Africa, and South America, where the model's amplitudes are 80, 84, and 200% larger, respectively, than those seen in the data. Smaller positive biases are found over southern Africa and Australia. At the same time, CCM3 tends to underestimate the amplitude of the diurnal cycle over some of the open oceans. This finding is consistent with the results for the later version of the NCAR model, CCSM2 [*Dai and Trenberth*, 2004]. Examples include the southwestern tropical Pacific, the northern tropical Atlantic, and the northwestern tropical Pacific Oceans where the amplitudes are 35, 39, and 57% smaller, respectively, than those seen in the data. In the model, the phase of the

**Table 1.** CCM3 Zone-Averaged Diurnal Cycle Relative To TRMM[a]

| Zone | Amplitude | Phase |
|---|---|---|
| NE tropical Pacific Ocean | similar | precedes by ~2 hours |
| SE tropical Pacific Ocean | similar | precedes by 3 hours |
| South America | 200% larger[b] | similar |
| N tropical Atlantic Ocean | 39% smaller | precedes by 3–4 hours |
| S tropical Atlantic Ocean | 69% smaller | precedes by 6–7 hours[c] |
| N Africa | 84% larger | precedes by 3–4 hours[d] |
| S Africa | 67% larger | precedes by 2–3 hours |
| S central Asia | 80% larger | 1–2 hours |
| S Indian Ocean | similar | precedes by ~2 hours |
| SE Asia | N/A | N/A |
| Maritime Continent | N/A | N/A[e] |
| Australia | 48% larger | precedes by ~4 hours |
| NW tropical Pacific Ocean | 57% smaller | precedes by 2–3 hours[f] |
| SW tropical Pacific Ocean | 35% smaller | precedes by 3–4 hours |

[a]Similar, an amplitude difference of less than 10% or phase difference of less than 1 hour; NA, not available.
[b]Largest in southeastern South America, region 9F.
[c]Large amount of uncertainty in TRMM fit here.
[d]Precedes by 9–10 hours in Saharan Desert region 13A.
[e]Precedes by 5–6 hours in Papua New Guinea, region 22D.
[f]Precedes by 10–11 hours in northwestern tropical Pacific region 21A.

diurnal harmonic consistently precedes the data in the majority of the regions we analyze. This finding is not inconsistent with the results of *Dai and Trenberth* [2004] for CCSM2, in which deep moist convection is found to initiate prematurely. Largest phase differences tend to occur over northern Africa (3 to 4 hours) and Australia (4 hours) as well as over the southern tropical Atlantic (6 to 7 hours), though there is a large amount of uncertainty in the fitting of the TRMM data over this last zone. Elsewhere, there are isolated regions where the model-satellite phase differences are significant. For example, the model's diurnal harmonic leads that of the data by 5 to 6 hours over Papua New Guinea and by nearly 10 to 11 hours over a region of the northwestern tropical Pacific.

[31] The strong forcing by the diurnal cycle of solar radiation provides an important test of the ability of climate models to simulate many processes in the climate system. The model-satellite differences detected in this study provide information that should be useful both for understanding the climatic role of convective processes and for improving parameterizations of surface and boundary layer processes and deep convection.

[32] **Acknowledgments.** This material is based upon work supported by a NASA Earth System Science fellowship and by NASA grant NAG5-4753 to Texas A&M University. The authors thank the Goddard Space Flight Center for making the TRMM satellite data available online via the TRMM Science Data and Information System; the Community Climate Model group at NCAR for developing and assistance with running CCM3; and the Program for Climate Model Diagnosis and Intercomparison at Lawrence Livermore National Laboratory for providing the sea-surface temperature data set in CCM3 format. The authors appreciate the guidance of Gerald North (Department of Atmospheric Sciences, Texas A&M University) and the assistance of H. J. Newton (Department of Statistics, Texas A&M University) with some of the statistical analysis. In addition, the authors thank the anonymous reviewers, whose insightful comments and suggestions helped bring this paper to publication.

## References

Albright, M. D., E. E. Recker, R. J. Reed, and R. Dang (1985), The diurnal variation of deep convection and inferred precipitation in the central tropical Pacific during January–February 1979, *Mon. Weather Rev.*, *113*, 1663–1680.

Anderson, T. (1978), *The Statistical Analysis of Time Series*, 704 pp., John Wiley, Hoboken, N. J.

Barnett, T. P. (1995), Monte Carlo climate forecasting, *J. Clim.*, *8*, 1005–1022.

Bell, T. L., and P. K. Kundu (1996), A study of the sampling error in satellite rainfall estimates using optimal averaging of data and a stochastic model, *J. Clim.*, *9*, 1251–1268.

Bell, T. L., and P. K. Kundu (2000), Dependence of satellite sampling error on monthly averaged rain rates: Comparison of simple models and recent studies, *J. Clim.*, *13*, 449–462.

Bell, T. L., and P. K. Kundu (2003), Comparing satellite rainfall estimates with rain gauge data: Optimal strategies suggested by a spectral model, *J. Geophys. Res.*, *108*(D3), 4121, doi:10.1029/2002JD002641.

Bell, T. L., P. K. Kundu, and C. D. Kummerow (2001), Sampling errors of SSM/I and TRMM rainfall averages: Comparison with error estimates from surface data and a simple model, *J. Appl. Metorol.*, *40*, 938–954.

Betts, A. K., and C. Jakob (2002a), Evaluation of the diurnal cycle of precipitation, surface thermodynamics, and surface fluxes in the ECMWF model using LBA data, *J. Geophys. Res.*, *107*(D20), 8045, doi:10.1029/2001JD000427.

Betts, A. K., and C. Jakob (2002b), Study of diurnal cycle of convective precipitation over Amazonia using a single column model, *J. Geophys. Res.*, *107*(D23), 4732, doi:10.1029/2002JD002264.

Brier, G. W., and J. S. Simpson (1969), Tropical cloudiness and precipitation related to pressure and tidal variations, *Q. J. R. Meteorol. Soc.*, *95*, 120–147.

Cess, R. (1985), Nuclear war: Illustrative effects of atmopsheric smoke and dust upon solar radiation, *Clim. Change*, *7*, 237–251.

Chang, A., L. Chiu, and G. Yang (1995), Diurnal cycle of oceanic precipitation from SSM/I data, *Mon. Weather Rev.*, *123*, 3371–3380.

Chen, M., R. E. Dickinson, X. Zeng, and A. N. Hahmann (1996), Comparison of precipitation observed over the continental United States to that simulated by a climate model, *J. Clim.*, *9*, 2233–2249.

Chervin, R. M. (1980a), On the simulation of climate and climate change with general circulation models, *J. Atmos. Sci.*, *37*, 1903–1913.

Chervin, R. M. (1980b), Estimates of first- and second-moment climate statistics in GCM simulated climate ensembles, *J. Atmos. Sci.*, *37*, 1889–1902.

Chervin, R. M. (1981), On the comparison of observed GCM simulated climate ensembles, *J. Atmos. Sci.*, *38*, 885–901.

Collier, J. C., K. P. Bowman, and G. R. North (2004), A comparison of tropical precipitation simulated by the NCAR Community Climate Model CCM3 with that observed by the Tropical Rainfall Measuring Mission (TRMM) satellite, *J. Clim.*, in press.

Cronin, M. F., and M. J. McPhaden (1999), Diurnal cycle of rainfall and surface salinity in the western Pacific warm pool, *Geophys. Res. Lett.*, *26*(23), 3465–3467.

Dai, A. (2001), Global precipitation and thunderstorm frequencies. part II: Diurnal variations, *J. Clim.*, *14*, 1112–1128.

Dai, A., and K. E. Trenberth (2004), The diurnal cycle and its depiction in the Community Climate System Model, *J. Clim.*, *17*, 930–951.

Dai, A., F. Giorgi, and K. E. Trenberth (1999), Observed and model-simulated diurnal cycles of precipitation over the contiguous United States, *J. Geophys. Res.*, *104*(D6), 6377–6402.

Ebert, E., and J. Curry (1992), A parameterization of ice cloud optical properties for climate models, *J. Geophys. Res.*, *97*, 3831–3836.

Gray, W. M., and R. W. Jacobson (1977), Diurnal variation of deep cumulus convection, *Mon. Weather Rev.*, *105*, 1171–1188.

Hack, J. (1994), Parameterization of moist convection in the National Center for Atmospheric Research Community Climate Model (CCM2), *J. Geophys. Res.*, *99*, 5551–5568.

Holtslag, A., and B. Boville (1993), Local versus nonlocal boundary-layer diffusion in a global climate model, *J. Clim.*, *6*, 1825–1842.

Janowiak, J. E., P. A. Arkin, and M. Morrissey (1994), An examination of the diurnal cycle in oceanic tropical rainfall using satellite and in situ data, *Mon. Weather Rev.*, *122*, 2296–2311.

Kiehl, J., J. Hack, G. Bonan, B. Boville, B. Briegleb, D. Williamson, and P. Rasch (1996), Description of the NCAR Community Climate Model (CCM3), *Tech. Rep. NCAR/TN-420+STR*, Natl. Cent. for Atmos. Res., Boulder, Colo.

Kiehl, J., J. Hack, G. Bonan, B. Boville, D. Williamson, and P. Rasch (1998), The National Center for Atmospheric Research Community Climate Model: CCM3, *J. Clim.*, *11*, 1131–1149.

Kirkyla, K. I., and S. Hameed (1989), Harmonic analysis of the seasonal cycle in precipitation over the United States: A comparison between observations and a general circulation model, *J. Clim.*, *2*, 1463–1475.

Kraus, E. B. (1963), The diurnal precipitation change over the sea, *J. Atmos. Sci.*, *20*, 551–556.
Kummerow, C., W. Barnes, T. Kozo, J. Shiue, and J. Simpson (1998), The Tropical Rainfall Measuring Mission (TRMM) sensor package, *J. Atmos. Oceanic Technol.*, *15*, 809–817.
Kummerow, C., et al. (2000), The status of the Tropical Rainfall Measuring Mission (TRMM) after two years in orbit, *J. Appl. Meteorol.*, *39*, 1965–1982.
Latif, M., et al. (2001), ENSIP: The El Niño simulation intercomparison project, *Clim. Dyn.*, *18*, 255–276.
Lin, X., D. A. Randall, and L. D. Fowler (2000), Diurnal variations of the hydrologic cycle and radiative fluxes: Comparisons between observations and a GCM, *J. Clim.*, *13*, 4159–4179.
Lindzen, R. S. (1981), Turbulence and stress swing owing to gravity wave and tidal breakdown, *J. Geophys. Res.*, *86*, 9707–9714.
Liou, K. (1992), *Radiation and Cloud Processes in the Atmosphere*, 487 pp., Oxford Univ. Press, New York.
Lorenz, E. N. (1963), Deterministic nonperiodic flow, *J. Atmos. Sci.*, *20*, 130–141.
McFarlane, N. (1987), The effect of orographically excited wave drag on the general cicrulation of the lower stratosphere and troposphere, *J. Atmos. Sci.*, *44*, 1775–1800.
McGarry, M. M., and R. J. Reed (1978), Diurnal variations in convective activity and precipitation during phases II and III of GATE, *Mon. Weather Rev.*, *106*, 101–113.
Meisner, B. N., and P. A. Arkin (1987), Spatial and annual variations in the diurnal cycle of large-scale tropical convective cloudiness and precipitation, *Mon. Weather Rev.*, *115*, 2009–2032.
Negri, A. J., and T. L. Bell (2002), Sampling of the diurnal cycle of precipitation using TRMM, *J. Atmos. Oceanic Technol.*, *19*, 1333–1344.
Nesbitt, S. W., and E. J. Zipser (2003), The diurnal cycle of rainfall and convectdive intensity according to three years of TRMM measurements, *J. Clim.*, *16*, 1456–1475.
Ramanathan, V. (1976), Radiative transfer within the Earth's troposphere and stratosphere: A simplified radiative-convective model, *J. Atmos. Sci.*, *33*, 1330–1346.
Ramanathan, V., and P. Downey (1986), A nonisothermal emissivity and absorptivity formulation for water vapor, *J. Geophys. Res.*, *91*, 8649–8666.
Randall, D. A., and D. A. Dazlich (1991), Diurnal variability of the hydrologic cycle in a general circulation model, *J. Atmos. Sci.*, *48*, 40–62.
Reed, R. J., and K. D. Jaffe (1981), Diurnal variations of summer convection over West Africa and the tropical eastern Atlantic during 1974 and 1978, *Mon. Weather Rev.*, *109*, 2527–2534.
Sharma, A. K., A. T. C. Chang, and T. T. Wilheit (1991), Estimation of the diurnal cycle of oceanic precipitation from SSM/I data, *Mon. Weather Rev.*, *119*, 2168–2175.
Shin, K.-S., and G. R. North (1988), Sampling error study for rainfall estimate by satellite using a stochastic model, *J. Appl. Meteorol.*, *27*, 1218–1231.
Slingo, J. (1987), The development and verification of a cloud prediction scheme for the ECMWF model, *Q. J. R. Meteorol. Soc.*, *113*, 899–927.
Slingo, J. (1989), A GCM parameterization for the shortwave radiative properties of water clouds, *J. Atmos. Sci.*, *46*, 1419–1427.
Taylor, K. E., D. Williamson, and F. Zwiers (2000), The sea surface temperature and sea-ice concentration boundary conditions for AMIP II simulations, *Tech. Rep. 60*, Program for Clim. Model Diagn. and Intercomp., Lawrence Livermore Natl. Lab., Berkeley, Calif.
Tracton, M. S., and E. Kalnay (1993), Operational ensemble prediction at the National Meteorological Center: Practical aspects, *Weather Forecast.*, *8*, 379–398.
Trenberth, K. E., A. Dai, R. M. Rasmussen, and D. B. Parsons (2003), The changing character of precipitation, *Bull. Am. Meteorol. Soc.*, *84*(9), 1205–1217.
Vogelzang, D., and A. Holtslag (1996), Evaluation and model impacts of alternative boundary-layer height formulations, *Boundary Layer Meteorol.*, *81*, 245–269.
Wallace, J. M. (1975), Diurnal variations in precipitation and thunderstorm frequency over the conterminous United States, *Mon. Weather Rev.*, *103*, 406–419.
Zhang, G., and N. A. McFarlane (1995), Sensitivity of climate simulations to the parameterization of cumulus convection in the Canadian Climate Centre general circulation model, *Atmos. Ocean*, *33*, 407–446.
Zhang, G. J., J. T. Kiehl, and P. J. Rasch (1998), Response of climate simulation to a new convective parameterization in the National Center for Atmospheric Research Community Climate Model (CCM3), *J. Clim.*, *11*, 2097–2115.

K. P. Bowman and J. C. Collier, Department of Atmospheric Sciences, Texas A & M University, College Station, TX 77843-3150, USA. (jcollier@ariel.met.tamu.edu)